

# Case study: Electric Skateboards

Telemetry Data Analysis

Semester Thesis

at the Department of Mechanical Engineering of Technical University of Munich

**Supervised by**

**Submitted by** Institute of Automotive Technology  
Mathias Recalde Koller, B.Sc.

**Submitted on** Garching, January 01, 2019



# Project description

## Case study: Electric Skateboards, telemetry data analysis

The goal of this thesis is to collect and analyze telemetry data generated from electric skateboards. In order to objectively evaluate the data, several different sources should be taken into account.

The following tasks must be completed by Mr. Mathias Recalde Koller:

- Collection of telemetry data.
- Preprocessing of the collected data.
- Processing of the data.
- Generation of a representative driving cycle.
- Evaluation of the results.

The composition of this work should be documented in a clear and precise form. The candidate commits to work on the semester thesis independently and to specify the scientific resources that were used.

Announcement date: June 1, 2018

---

Submission date: January 1, 2019

---



## Erklärung

Ich versichere hiermit, dass ich die von mir eingereichte Abschlussarbeit selbstständig verfasst und keine anderen als die angegebenen Quellen und Hilfsmittel benutzt habe.

Hereby I assure that the thesis I submitted was independently written and no resources other than the cited ones were used.

Garching, den 1. Januar 2019

---

Mathias Recalde Koller, B. Sc.



# Contents

<b>Formula Symbols</b> .....	<b>III</b>
<b>1 Motivation and Goals</b> .....	<b>1</b>
<b>2 Problem Background</b> .....	<b>3</b>
<b>2.1 Micro-Mobility</b> .....	<b>3</b>
<b>2.2 Electric Skateboards</b> .....	<b>3</b>
2.2.1 Relevant Components.....	4
2.2.2 Current Regulative Situation.....	8
2.2.3 Tracking Apps.....	8
<b>3 State of the Art</b> .....	<b>11</b>
<b>4 Approach</b> .....	<b>15</b>
<b>4.1 Data Management</b> .....	<b>16</b>
<b>4.2 Data Analysis</b> .....	<b>20</b>
<b>4.3 Driving-Cycle Generation</b> .....	<b>20</b>
<b>5 Results</b> .....	<b>23</b>
<b>5.1 Driving Behavior</b> .....	<b>23</b>
<b>5.2 Use of Energy</b> .....	<b>26</b>
<b>5.3 Driving Cycle</b> .....	<b>28</b>
<b>6 Discussion</b> .....	<b>37</b>
<b>7 Conclusion</b> .....	<b>39</b>
<b>List of Figures</b> .....	<b>i</b>
<b>List of Tables</b> .....	<b>iii</b>
<b>Bibliography</b> .....	<b>v</b>
<b>Appendix</b> .....	<b>vii</b>





# Formula Symbols

Formula Symbols	Unit	Description
$x$	m	Distance
$D_{\text{Wheel}}$	m	Wheel diameter
$i$	-	Gear ratio
$a_x$	m/s <sup>2</sup>	Longitudinal acceleration
$v$	m/s	Speed
$\mu$	-	Population mean
$T$	s	ESC update interval
$\sigma$	-	Population standard deviation
$\Lambda$	-	Pearson distribution type
$M$	Nm	Torque
$f_1$	Hz	Electrical motor frequency
$p$	-	Motor pole-pairs
$i_s^q$	A	q-axis stator current
$\Psi_{PM}^d$	Wb	d-axis permanent magnet magnetic flux
$I$	A	Current
$R$	$\Omega$	Electrical resistance
$C_{\text{Battery}}$	Ah	Battery capacity
$C_{\text{Load}}$	F	Load capacitance
$P$	W	Power



# 1 Motivation and Goals

Urban mobility has become one of the most significant challenges of this century. As cities keep growing and evolving quicker than their road and public transport infrastructures, several noteworthy problems have emerged. Trains and subways struggle to meet up with peak-hour demand, resulting in a stressful and uncomfortable ride for the passengers. Those who instead opt to commute by car often find themselves stuck in a traffic congestion and then struggle with insufficient parking options.

The before mentioned growth has resulted in urban areas with a high density of internal-combustion-engine (ICE) vehicles, which combined with household heating and other local pollutants have deteriorated the local air quality. The 2018 air quality report by the European Environment Agency (EEA) [1] states that, according to 2016 data, as much as 98 % of the total EU-28 urban population was exposed to ozone levels exceeding the World Health Organization (WHO) air quality guidelines [2]. They also state that the exposure to fine particulate matter ( $PM_{2.5}$ ), ozone ( $O_3$ ), and nitrogen dioxide ( $NO_2$ ), all byproducts of the combustion process of ICE-cars, may lead to adverse health effects, such as morbidity and premature mortality. The mortality expectancy is mainly related to respiratory and cardiovascular diseases.

One of the possible solutions to transportation and environmental problems are personal light electric vehicles (PLEV). They do not emit  $PM_{2.5}$ ,  $NO_2$ ,  $O_3$ , or any other local pollutants, are highly accessible, and their total volume is almost negligible when compared to an average car. This type of transportation offers the same kind of flexibility as a car, since it will always remain accessible, unlike public transport systems that follow fixed schedules. Moreover, it has been proven that even modest increases in alternative personal transport may confer physical activity, health and environmental benefits [3].

This thesis aims to analyze the usage of these transportation devices, not based on synthetic theoretical data but rather on real-world information. One possible solution is to perform a case study where participants from all over the world provide their ride telemetry, similar to the work published by Bishop et al. [4] on electric scooters. A world-wide case study is not subjected to particular environmental situations, physical rider size nor driving style.

The focus of this work is set on electric skateboards. An e-skateboard is a battery-powered mobility device that is driven by an electric motor, typically a small sized permanent magnet synchronous outrunner machine, which is controlled by a hand-held wireless remote or weight sensing pads that act as throttle input when shifting the body weight. The electric motors both accelerate and decelerate the skateboard as they generate a counter force when switched into a regenerative operation mode.

The data-samples analyzed in this case study are provided by several users of an online forum dedicated to building custom electric skateboards [5]. Thanks to the open-source platform of the electric speed controller (ESC) that is used by the participants, it is possible to share ride-telemetry combined with GPS speed and altitude information collected via their mobile-phone

devices. The usage of smart-phones as tracking devices has enabled the realization of many case studies without requiring large telemetry equipment investments. Jäger et al. for example used smart-phones as tracking devices to study the supply and demand of a taxi network.

These are the main objectives of this thesis:

- **Collection of the telemetry data:**

The case study data is provided by anonymous users from around the world.

- **Preprocessing of the collected data:**

Due to the heterogeneity of the data sources the telemetry structure is converted to a common form for easier evaluation.

- **Processing of the data:**

The collected data is statistically analyzed to understand the usage of e-skateboards.

- **Generation of a representative driving cycle:**

Creation of a representative driving cycle based on the collected data. An e-skateboard specific driving cycle has the potential to be used as a tool for further development of e-skateboard related scientific work.

- **Evaluation of the results**

Critical discussion of the presented results. Possible problem solutions or improvement requirements may be suggested.

## 2 Problem Background

In order to obtain a better understanding of the general subject, information regarding e-skateboards is presented in the following section.

### 2.1 Micro-Mobility

Micro-Mobility, often referred to as last-mile-transportation, describes the movement of goods or people from a transportation interchange to a final destination such as a workplace, meeting-location or home [6].

Public transport networks are composed of a quite complex bus- and train-network. However, they often lack flexible *door-to-door* mobility services, which compromises the overall efficiency of a typical commute.

Personal light electric vehicles such as e-skateboards can help solve that last link in the commute chain. Skateboards can easily be carried in subways, trains, and even buses. Thanks to the electrification, e-skateboards offer an effortless transportation experience. They even improve vehicle control and stability when compared to regular skateboards that lack an integrated braking solution. Since they are electric they also do not contribute to the local air pollution.

### 2.2 Electric Skateboards

Electric skateboards were earlier defined in Section 1 as battery powered electric vehicles which are operated with a wireless remote or weight sensing pads. Like all other e-mobility vehicles, they consist of four key components: a traction battery, a battery management system (BMS) or an equivalent protection circuit module (PCM), an electric speed controller (ESC), and one or more electric motors.

What differentiates skateboards from other EVs is the kinematic system, as the turning is not performed by a steering wheel or handlebar but rather by shifting the riders body weight.

In the following subsection the before-mentioned components are briefly described, as they play a crucial role in energy consumption and power generation. Due to the lack of specific literature some statements are based on personal experience. E-skateboards are a relatively new concept that has not been investigated as extensively as other mobility devices.

The above-named components can be found in Figure 2.1: ESC (1), battery (2), remote control receiver (3), Bluetooth Low Energy BLE-Module (4), BMS (5), motor and mechanical drive-train (6).

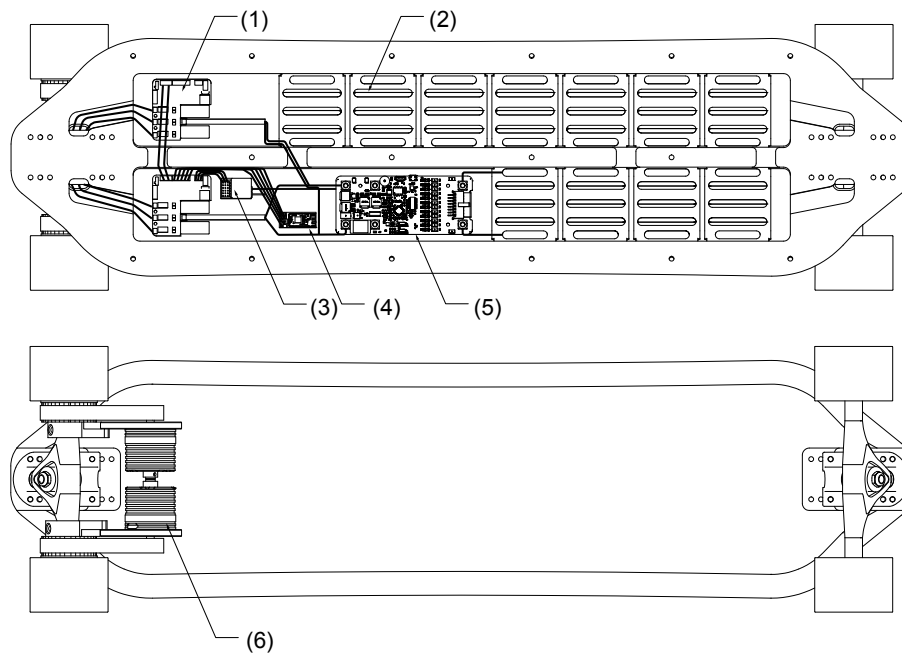


**Figure 2.1.** Electric skateboard

### 2.2.1 Relevant Components

#### ESC

One of the essential components of this case study is the electronic speed controller. All the collected telemetry data is processed and transmitted through that device. The controller type used by the participants of this study is denominated VESC, or Vedder-ESC, named after its creator, the Swedish engineer Benjamin Vedder [7].

The VESC<sup>®</sup> is a compact sized open source controller that was explicitly designed for small electric vehicles such as e-skateboards, e-bikes or even electric motorcycles in the lower power spectrum. The current ratings vary depending on the hardware version, ranging from maximum continued ratings of 50 to 80 A. The MOSFET gate driver, DRV8302 or DRV8302, rated up to 60 V, constrains the voltage rating of the ESC.

The technical drawing presented in Figure 2.2 shows both V6 (65x65 mm) and V4 (120x45 mm) architectures. The main differences are the L-Shaped PCB (2), DirectFET<sup>®</sup> MOSFETs (2) for better heat transfer, and three shunt current amplifiers instead of two (3). All these changes were introduced to improve the stability and reliability under field-oriented control (FOC); especially running under higher voltage.

The ESC hardware and software support both square wave- and FOC commutation [8]. The latter being the preferred choice as a result of the higher overall electrical efficiency, better torque generation and a much lower pitch sound than the usually generated over square wave commutation. K. H. Nam explains this phenomenon in detail in his study [9].

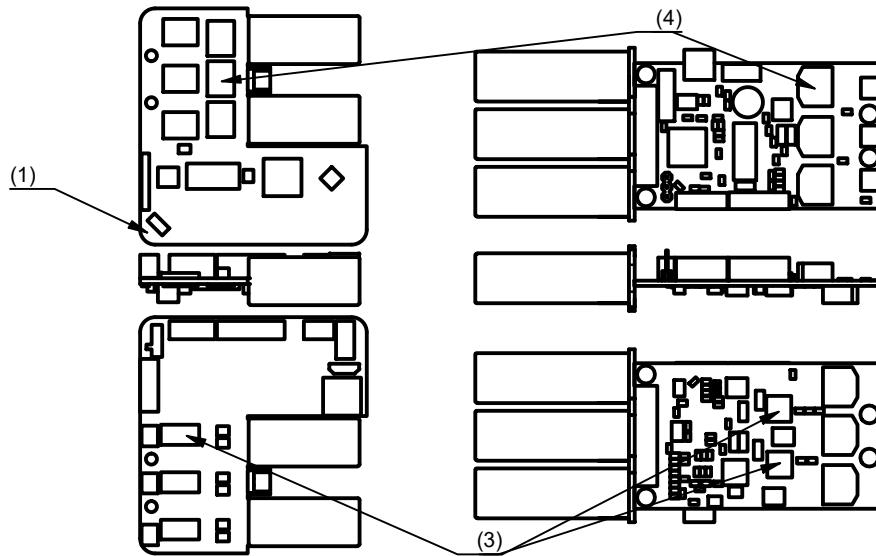


Figure 2.2. VESC design: left: V6; right: V4

## Battery

An array of Lithium-ion battery cells powers almost every e-skateboard: mostly standardized cylindrical 18650 or 20700 cells, lithium-ion polymer pouch-cells (*LiPo*) or either prismatic or cylindrical Lithium iron phosphate cells (*LiFePO<sub>4</sub>*).

Due to the excellent modularity, power- and energy-density capabilities, Li-Ion cylindrical cells are the preferred choice for light electric vehicles. The first two digits of the standardized naming represent the cell diameter in mm, and the last three digits represent the length in 0.1 mm.

Because of the high-power demand relative to the battery size, Li-Ion NMC (*LiNiMnCoO<sub>2</sub>*) or LMO (*LiMn<sub>2</sub>O<sub>4</sub>*) chemistry types are commonly utilized. Yuan et al. [10] state that the addition of manganese to the battery cathode oxide allows the cell to be discharged at a higher current whilst maintaining lower temperatures when compared to high energy chemistry types such as NCA (*LiNiCoAlO<sub>2</sub>*).

High-power lithium-ion cylindrical batteries are typically rated for 3 C to 6 C continuous discharges, that means a maximum current output  $I_{MAX}$  of 3 to 6 times its maximum capacity  $C$  (2.1). High-power lithium-ion-polymer batteries present much higher discharge ratings, often exceeding C-Ratings of 50 C.

$$\text{C-Rate} = \frac{I_{MAX} \cdot h^{-1}}{C_{Battery}} \quad (2.1)$$

Lithium-ion batteries are usually rated for 1C continuous charging due to the the higher internal resistance when charging [10], a value two to five times lower than the discharge rating. This asymmetry can be observed when comparing common absolute charge and discharge ESC-settings. A workaround to allow higher regenerative braking-current is to use of a brake resistor that absorbs the excess current that the battery cannot handle.

As mentioned before, the maximum voltage rating of the ESC gate-driver is 60V. Therefore, serial connections up to 13 cells (13S) are used in this case study.

### BMS

A battery management system or BMS is an electronic control system that monitors and protects single cells or battery cell-arrays. Typical tasks for a BMS are over- and under-discharge protection, over-current protection, cell balancing, and short-circuit protection. Some more advanced functions include temperature protection, state of health (SOH) and state of charge (SOC) monitoring, as well as communication to other electronic systems such as the ESC.

The MOSFETS and the cooling system used in the BMS typically dictate the maximum current output, which usually matches the expected maximum constant current input to the ESCs.

Another feature many battery management systems include is the integration of an electronic start switch (e-switch), commonly referred to as an *anti-spark-switch*. Because of the high inrush current generated by the battery, a dedicated system powering solution is needed in order to protect the components attached to the battery from overcurrent damage.

The inrush current is generated when a capacitive load (ESC-Capacitors) is switched onto a powerrail (e-skateboard battery), and must be charged to that voltage level. The amount of inrush current into the capacitors is determined by the slope of the voltage ramp as described in (2.2):

$$I_{Inrush} = C_{Load} \cdot \frac{dV}{dt} \quad (2.2)$$

$C_{LOAD}$  refers to the total capacitance of the ESC capacitors,  $dV$  to the change in voltage during ramp-up, and  $dt$  to the rise time during voltage ramp-up.

### Motor

Permanent magnet synchronous AC motors (PMSM) are almost exclusively used in light electric vehicle applications due to the excellent power to weight ratio, torque density and high-efficiency rating [11]. Out of the possible two PMSM variants, outrunners are mainly used in e-skateboards. This type of motor rotates its outer shell around its windings. One of its benefits is the forced convective-cooling generated by the outwards located rotor, which helps combating magnetic flux saturation at higher temperatures.

Figure 2.3 shows an exploded assembly drawing of a direct drive hubmotor from ENERTION<sup>®</sup>. Numbered from left to right are the copper filled stator, permanent magnets, rotor-can, and the polyurethane outwheel that contacts the road surface.

### Mechanical Drive-Train Components

Besides its electric drive-train components, e-skateboards are composed of a variety of non-electric parts that affect its kinematics and also influence the energy consumption ( $E_C$ ). The most relevant components are the steering trucks, wheels, and the drive-train transmission type.

Due to the increased stability and control, Reverse-King-Pin (RKP) trucks are utilized typically on e-skateboards, which normally use longer decks with an increased wheelbase. Figure 2.4 (a) shows the geometry of an RKP-Truck, where the kingpin, on which the truck pivots, faces the outside of the deck, contrary to traditional kingpin trucks (TKP), where the king-pin is oriented inwards. A higher truck angle, also shown in Figure 2.4 (a), results in a shorter turning radius.



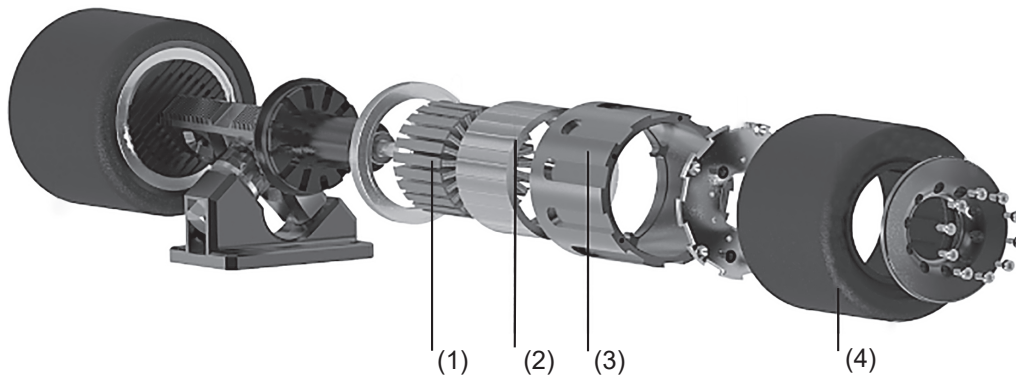


**Figure 2.3.** ENERTION® direct drive hubmotor.

Figure 2.4 (b) shows the influence of positive rake on the turning radius-lean curve: the result is a more progressive response curve that often helps when riding at higher speeds, as small involuntary leans do not destabilize the board.

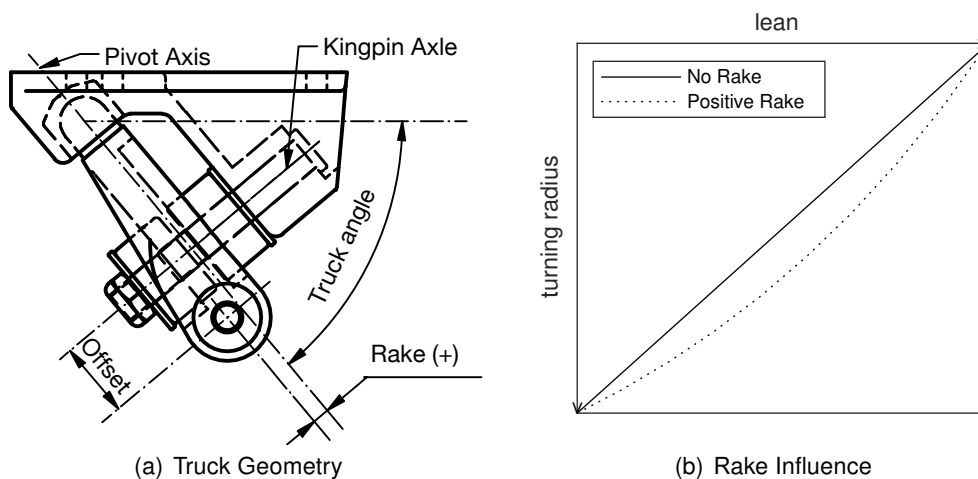


**Figure 2.4.** RKP truck kinematics

As far as wheel choice goes, polyurethane wheels, sized 70 to 110 mm in diameter, or pneumatic wheels, sized 5 to 8", are utilized on e-skateboards. Due to the much worse energy efficiency of pneumatic wheels only polyurethane wheels, which are designed for urban conditions, are used in this case study. E-skateboards with larger diameter wheels often present a higher consumption value due to the added rotational mass when accelerating. The shore hardness of the wheels used ranges typically between 70a and 90a: softer wheels provide more grip and offer generally a more comfortable ride.

The third and last-mentioned component, the transmission, also plays a key role in the overall energy efficiency of the drive-train. Usually either a timing belt driven system or a direct drive solution is used. The 1:1 gear-ratio direct-drive system being the less efficient, caused by the increased current when accelerating. As shown in (2.3) and (2.4), the generated torque is proportional to the current and the ohmic power-losses are proportional to the square of the current [9]. A geared drive train system with a 1:3 gear ratio would require one third of the

startup-current, as the q-axis stator current  $i_s^q$  is the only non-fixed variable in (2.3). This would result in nine times lower power-losses than a comparable direct-drive system.

$$M_{PMSM} = \frac{3}{2} p \cdot \Psi_{PM}^d \cdot i_s^q \quad (2.3)$$

$$P \propto I^2 \cdot R \quad (2.4)$$

### 2.2.2 Current Regulative Situation

As of late 2018 self-propelled electric vehicles lack specific regulations in most countries around the world. As a result, they are often classified as automobiles and are therefore illegal to ride in public spaces.

Some more progressive countries such as Sweden [12], Finland [13], Singapore [14], and US-American states such as California [15] have already approved regulations either targeted to PLEVs or e-skateboards directly.

In most cases the regulations impose a maximum ride speed: for example 32 km/h in California or 25 km/h in Singapore. Sometimes a power limitation is mandated too, for instance 1 kW in California.

### 2.2.3 Tracking Apps

It was briefly mentioned in Section 1 that the data-source of this case study was ride-telemetry provided by anonymous users around the world. The data-logging is done by mobile apps that communicate to the ESC. The applications connect to the ESC via Bluetooth® low energy (BLE); Usually to an nRF52 or HM-10 master-slave 2.4 GHz module connected to the VESC® UART output port.

All relevant telemetry variables are collected:

- Motor- and battery-current
- Electrical motor frequency ( $f_1$ )
- Voltage
- Duty-cycle
- ESC- and motor-temperature
- Ampere-hours discharged and charged
- Watt-hours discharged and charged
- ESC fault codes
- Time-step for every appended data-point

The collected data is merged with the GPS speed, longitude, latitude and altitude data-points that are provided by the tracking mobile phone.

If the user disabled the localization data, the speed telemetry is calculated according to (2.5):

$$v = \frac{f_1}{p} \cdot \pi D_{wheel} \cdot i \quad (2.5)$$

In order to calculate the ride speed the electrical motor frequency  $f_1$  is divided by the motor pole-pair  $p$ . This delivers the mechanical rotational speed of the motor in Hz. Then the rotational speed is multiplied with the wheel perimeter  $\pi D_{wheel}$  and the gear ratio  $i$ .

Telemetry-data from three different tracking apps is used in this case study:

- **METR**<sup>®</sup>: developed by Roman Pasichnyk. Available on iOS and Android platforms.
- **eSkate-VESC**<sup>®</sup>: developed by Emmanuel Cordente. Available only for iOS .
- **ACKMANIAC-ESC Monitor**: developed by Nico Ackermann. Available only for the Android mobile operating system.



## 3 State of the Art

In the following chapter state of the art information regarding the approach of this case study is shown. Mainly information regarding driving cycle generation and statistical distribution analysis.

### Driving Cycle Generation

A Driving Cycle (DC) is a predefined discrete function of speed over time. It is used by vehicle manufacturers and traffic associations as a tool to determine vehicle energy consumption and tailpipe emissions in case the tested vehicle uses an internal combustion engine. It can be also purposed for product development and testing.

There are two main strategies for the creation of driving cycles:

- A theoretical approach:  
One example is the New European Driving Cycle (NEDC) [16]. The speed profile of the NEDC is rather rectangular, as it presents sections with constant acceleration/deceleration as well as sections with constant speed. These driving dynamics rarely represent under real-world conditions.
- A real-world ride-data based approach:  
The Worldwide harmonized Light vehicles Test Procedure (WLTP) [17] or the US-American Federal Test Procedure FTP-75 DC [18] are driving cycles based on real-world data. Strategies based on this approach represent longitudinal vehicle dynamics much better.

One of the objectives of this case study is to create a driving cycle tailored to e-skateboards. Analogue to the driving cycles developed for automobiles, an e-skateboard DC could be utilized to determinate realistic range estimations. Additionally it could also be used as a development platform.

Three different state of the art methods to generate driving cycles based on real word data were studied:

- Micro-trip combination method [19]:  
A representative driving cycle is generated by combining segments of real-world ride data. This stochastic approach works by generating a high number of possible DC candidates that are later compared to statistical parameters calculated out of real-world driving situations.
- DC generation with a parametrized tool [20]:  
Similar to the approach above, driving cycles are synthetically created by a tool

whose key parameters are statistically described.

- Method based on Markov Chain Monte Carlo (MCMC) [21]:

This approach is also based on stochastic methods: a representative DC is created by utilizing the properties of Markov Chain Monte Carlo algorithms. The driving cycle is usually modeled after a target route with fixed distance and speed constraints.

The first proposed method was chosen for the generation of a representative DC. It requires the least amount of parameters and constraints to be implemented correctly and still provides an acceptable representative value.

This proposed method consists on creating a large number of combinations of a set number of micro-trips, defined as the interval with nonzero ride speed between two stops. The generated driving cycles are then analyzed and evaluated according to relevant statistical parameters such as the mean and standard deviation values of speed and acceleration data-points, the proportions of idling-, creep-, cruise-, acceleration- and deceleration-time, as well as data probability distribution analysis.

To analyze speed and acceleration data distributions, discrete probability-distribution classification-methods were studied. The Pearson probability distribution method was chosen as it includes most common distribution types; for example Gaussian, Gamma, Beta, and Student's t-distributions. The system was introduced by Karl Pearson (1895), who worked out a set of four-parameter probability density functions [22]. The Pearson system utilizes statistical moments, which offer a quantitative measure of the shape of a distribution.

The first four normalized moments are defined by Montgomery et al. as follows [23]:

- Mean: the normalized mean value is always set to equal zero.
- Variance: the second normalized moment is one, because it is equal to the second power of the standard deviation  $\sigma = 1$ . The standard deviation quantifies the amount of variation of a set of data values.
- Skewness: the skewness is a measure of the asymmetry of the probability distribution.
- Kurtosis: the kurtosis describes the shape of a distribution, it refers to the "sharpness" of the function curve at its peak region.

The Pearson diagram, see Figure 3.1, relates the square skewness  $\beta_1$  to the traditional kurtosis  $\beta_2$  [24]:

$$\beta_1 = \frac{\mu_3^2}{\mu_2^3}, \quad \beta_2 = \frac{\mu_4}{\mu_2^2}, \quad (3.1)$$

where  $\mu_k$  is the  $k^{\text{th}}$  normalized moment for discrete data given by

$$\mu_k = \frac{1}{N\sigma^k} \sum_{i=1}^N [p_i - \mathbb{E}\{\mathcal{P}\}]^k = \frac{1}{N} \sum_{i=1}^N \left\langle \frac{[p_i - \mathbb{E}\{\mathcal{P}\}]}{\sigma} \right\rangle^k, \quad (3.2)$$

where  $\mathcal{P}$  is a finite subset of experimental data, and  $\sigma$  is the standard deviation of this subset.  $p_i$  refers to a sample observation from  $i = 1$  to  $N$ .  $\mathbb{E}$  is the expected value of the subset  $\mathcal{P}$ .

Figure 3.1 illustrates the different regions for Pearson distribution types I to VI. The upper white region shows an area in which combinations of  $\beta_1$  and  $\beta_2$  are not possible.

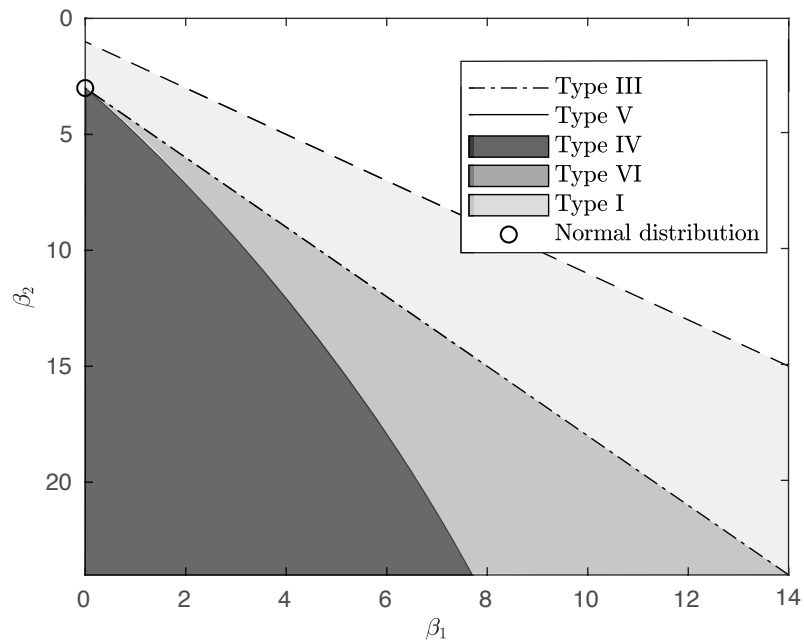


**Figure 3.1.** Pearson system distribution types





# 4 Approach

Figure 4.1 shows a simplified process diagram of the case study approach. The general approach can be segmented into three different layers: empiric foundation, preprocessing and finally evaluation. The first layer represents the initial step, where the case study participants submit their ride data via e-mail. The second section shows the data preparation and its different stages within the process; from the data collection until it gets prepared over MATLAB®. The final layer represents the analysis and evaluation of the preprocessed data.

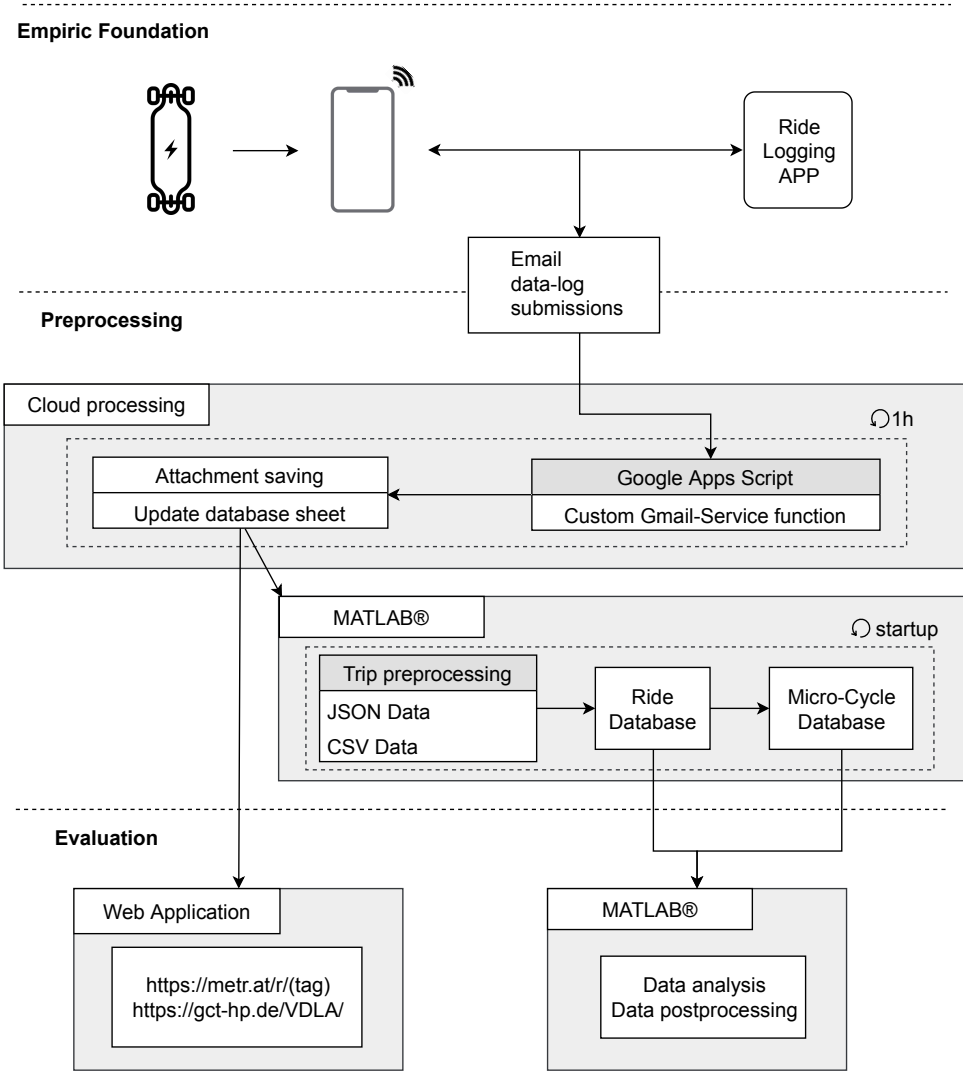


Figure 4.1. Overall process of the case study approach

## 4.1 Data Management

The following section describes the different steps that telemetry-data has to undergo before it gets analyzed.

### Telemetry Collection and First Preprocessing Step

The very first chain link in the overall process consists of recording the ride telemetry-data of a broad spectrum of different users. This is achieved thanks to the different data-logging apps that were mentioned in section 2.2.3 and a wireless data transmission interface connected to the ESC. The recorded data is then submitted via e-mail. The dots marked in Figure 4.2 show the different locations from where the data was submitted.

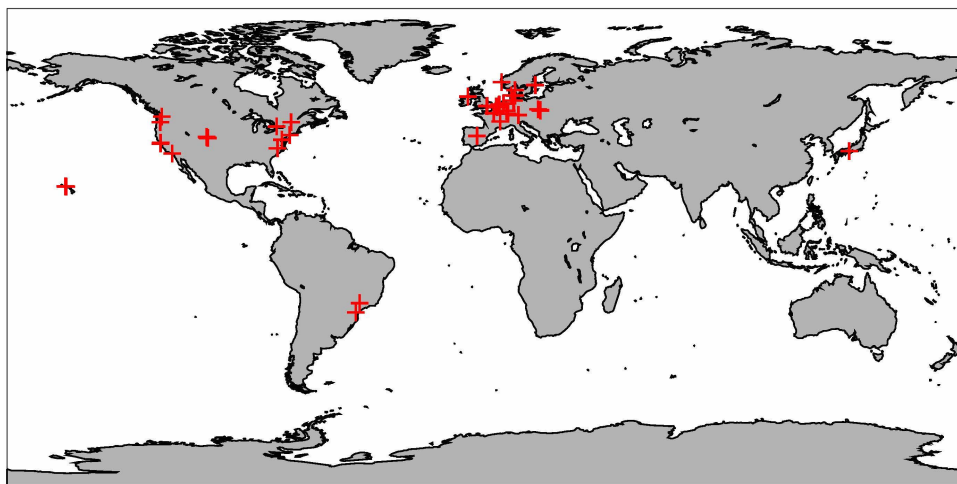


Figure 4.2. Data localization

To effortlessly manage the case study database, every data-preparation step is automated. First, a custom data scraping function, written within the Google Scripts cloud platform, extracts the relevant information out of the submitted e-mails. The Google Apps Script is a scripting language for simple app-development. Based on JavaScript 1.6, it provides a subset of functions that allow an easy automation across Google products [25].

The core functions of the data scraping script consist of saving the sent CSV log-files, METR<sup>®</sup> app ride-URL-links, and the provided rider information inside a Google-Docs sheet. The function work-flow is shown in Figure 4.3: when a new e-mail containing telemetry data is sent, it gets marked on the mail-client. Every hour the program executes and processes the e-mails that were marked. After unmarking, the program scrapes the email text and decides to proceed if the rider provided their weight information. After that there are two main work-flows depending on the data format. Finally the collected data gets saved in a common database sheet.

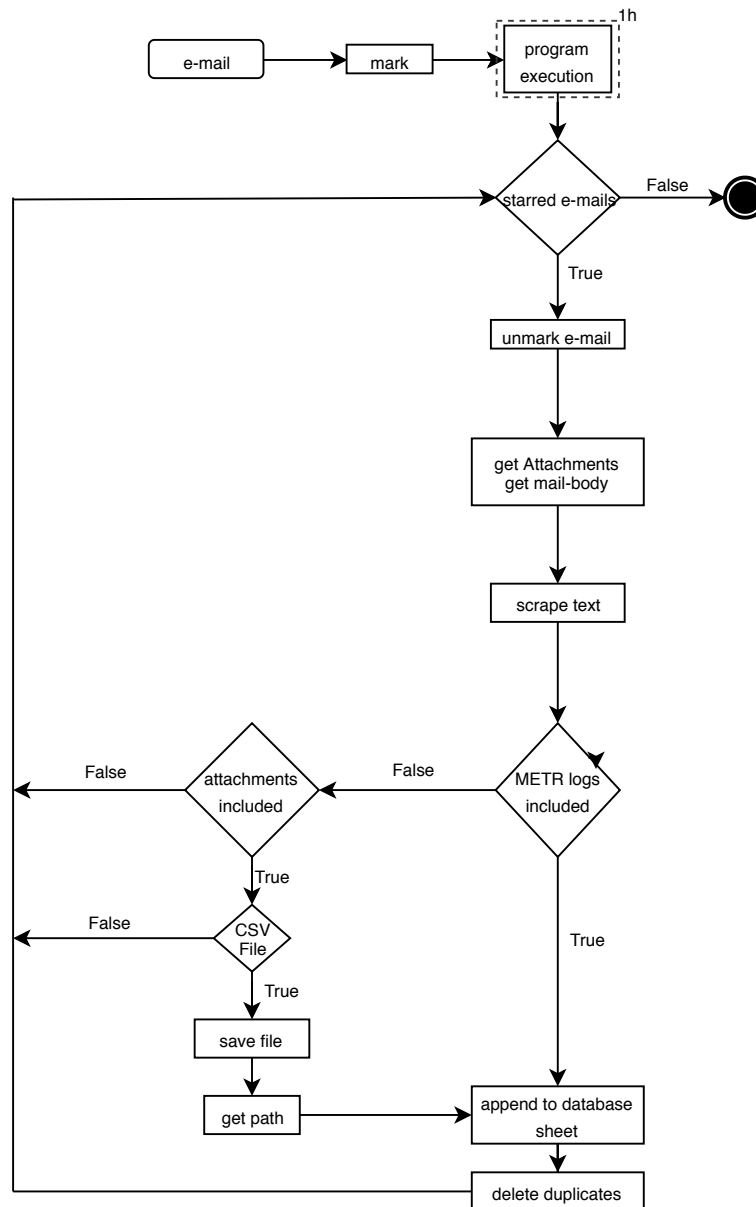


Figure 4.3. E-Mail scraper program work-flow

## Second Preprocessing Step

The second data preparation step consists of generating a unified database. A custom script executed locally in MATLAB® updates the database if new files were appended to the online log-sheet.

The script operates as follows: First, raw data-logs are converted to a unified structure. Then outlier entries and possibly damaged files are filtered out. Finally, the trips are segmented into micro-cycles and appended to a separate micro-cycle database.

Work-flow of the second preprocessing step:

- **1. Conversion of the Raw Data:**

The logs of two of the tracking apps mentioned in section 2.2.3, eSkate-VEESC® and ACKMANIAC-ESC Monitor, share the same CSV formatting, which is designed

for further online data visualization [26]. This data-structure was chosen as the reference structure for the final conversion and storage.

The following changes are implemented into the data-structure:

- The recorded time-stamps are converted to a standard universal UNIX format.
- String values are converted or removed to simplify CSV data reading.
- GPS longitude and latitude data is removed to guarantee user privacy.

Unlike the other apps, METR<sup>®</sup> app data is shared in form of a URL link that can be converted to JSON format. The before-mentioned preprocessing script reads the different variables stored in JSON-fields and places them inside a data matrix with the unified structure.

Some older app-version telemetry-logs lack information of charged watt-hours (Wh), motor temperature and ESC-count. Charged watt-hours can be calculated as shown in (4.1):

$$E_{regen} = \sum V \cdot I \cdot T \quad \forall \quad I < 0 \quad (4.1)$$

- **2. Data Error Correction:**

After the raw data is converted to a common structure, speed data-point errors are filtered out as can be observed in Figure 4.4. The time-stamp progression is also analyzed to detect unusually large update-periods that might happen if the user stopped the tracking of the ride and then resumed it afterward. Files presenting unrealistic consumption or distance end-values are also removed from the database.

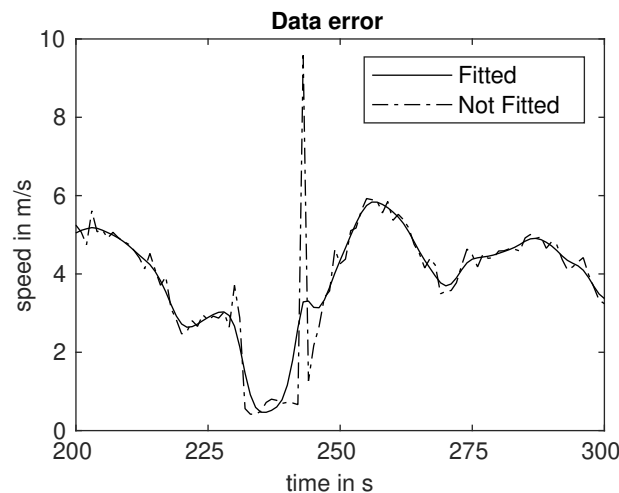


**Figure 4.4.** Speed data fitting

In order to clean the irregular speed data, a smoothing spline is utilized. As shown in (4.2), the smoothing spline  $s$  is constructed for the specified smoothing parameter

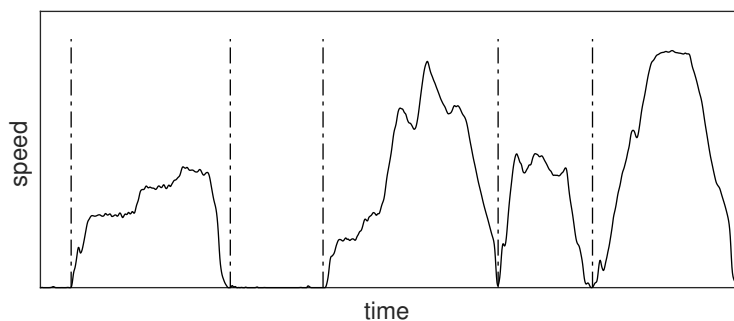
$p$  and the specified weights  $w_i$ :

$$p \sum_i w_i (y_i - s(x_i))^2 + (1 - p) \int \left( \frac{d^2 s}{dx^2} \right) dx \quad (4.2)$$

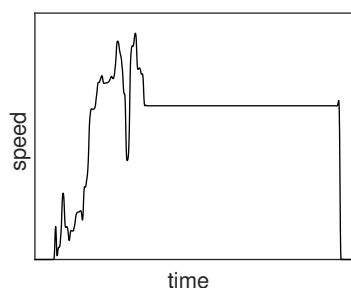
$p$  is defined between 0 and 1:  $p = 0$  produces a rougher least-squares straight-line fit to the data, while  $p = 1$  produces a smoother cubic spline interpolant. A value of  $p = 0.21$  was found to be sufficient. No weighting parameters  $w_i$  are needed, so they are assumed to equal 1 for all data points.

### • 3. Micro-Cycle Generation:

After filtering and data correction, the logs are segmented into micro-cycles. Micro-cycles were earlier defined in 3 as the interval with a positive ride speed between two stops. Intervals with a duration shorter than five seconds and or average speed smaller than 1.5 km/h are ignored due to GPS data-noise. Phases with long periods of constant speed are also rejected as such phenomena rarely present under real-world riding situations. Such a log-section with zero acceleration  $a_x = 0$  is pictured in Figure 4.5 (b). Figure 4.5 (a) shows an example of a segmented trip.



(a) trip segmented in micro-cycles



(b) rejected Micro-Cycle

**Figure 4.5.** Micro-Cycles

## 4.2 Data Analysis

The main goal of this case study is to analyze the general rider behavior and usage of their e-skateboards. Broad aspects such as trip distance, power usage, average speed, and energy-consumption are examined.

In order to analyze the collected data, probability distributions of the key parameters mentioned before are examined. Aspects such as average-, median- or standard-deviation-results showcase the general data response. In some cases, 3D-distributions or heatmaps are proven to be more useful when comparing two-dimensional data such as the correlation between speed and power or acceleration. In addition, the effect of characteristics such as mean speed, acceleration or altitude change on the energy consumption distribution shape is also examined.

Because of the heterogeneity of electrical drive-train setups used by the case study candidates, electrical parameters besides power usage are not analyzed. Battery configuration, motor, ESC-configuration and several other components have a considerable effect on the recorded electrical data. Therefore, a valid test would only be feasible if very similar setups were used.

## 4.3 Driving-Cycle Generation

The goal set for the generated driving cycles is to obtain the best possible representation of the collected real-world data. The employed micro-cycle combination method works as follows: a large set containing random combinations of real micro-cycles is created and then statistically analyzed. The statistical analysis is done by comparing fundamental parameters such as mean and standard deviation values of the speed and acceleration distributions as well as by comparing the Pearson distribution type of the generated DCs with the general distribution type.

Most parameters are based upon the decisions taken by Pfriem et al. [19], Hung et al. [27], Tong et al. [28], and Barlow et al. [29]. In addition to those parameters, the Pearson distribution system presented on Section 3 is added to the decision making process. By comparing the normalized distribution type of the candidate DCs with the distribution type of the collected data, the accuracy of the approach is further enhanced.

The list of parameters can be observed in Table 4.1:

**Table 4.1.** Overview of the parameters used for the DC-generation

No.	Parameter	Unit
1	Mean $v$	km/h
2	Mean positive $a_x^+$	m/s <sup>2</sup>
3	Mean negative $a_x^-$	m/s <sup>2</sup>
4	Acceleration RMS $a_x$	m/s <sup>2</sup>
5	Standard deviation $\sigma$ of $v$	-
6	Standard deviation $\sigma$ of $a_x$	-
7	Pearson distribution type $\Lambda_v$	-
8	Pearson distribution type $\Lambda_{a_x}$	-
9	Creeping proportion	%
10	Cruising proportion	%
11	Acceleration proportion	%
12	Deceleration proportion	%

The constraints to determine the percentile rank of the operation modes numbered 9 to 12 in Table 4.1 are shown in the Table below:

**Table 4.2.** Operating mode determination boundaries

Operating mode	Speed $v$ in km/h	Longitudinal acceleration $a_x$ in $m/s^2$
Idling	$v = 0$	$a_x = 0$
Cruising	$v > 7.2$	$0.01 \leq a_x \leq 0.01$
Creeping	$0 < v \leq 7.2$	$-0.01 \leq a_x \leq 0.01$
Acceleration	$v > 0$	$a_x > 0.01$
Deceleration	$v > 0$	$a_x < -0.01$

Work-flow of the employed DC-generator:

- **Step 1:**

Generation of a data-set containing  $10^6$  driving-cycle samples: the number of combined micro-cycles is set to be the median value of micro-cycles per trip. Because of the very high negative skewness of the distribution, the median value is chosen over the mean value.

- **Step 2:**

First filtering criterion: comparison of the initial eight parameters of Table 4.1 of the overall speed- and acceleration distribution with the values of the generated driving cycles. The parameter values, with exception of the Pearson distribution type, are rounded off to the nearest 0.05 increment. Samples with matching parameters are selected for further analysis in the next selection step.

- **Step 3:**

Second filtering criterion: comparison of the cruise-, creep-, acceleration-, and deceleration-proportions of the overall trip-distribution, numbered 9 to 12 in Table 4.1, with the proportions of the filtered candidates after step 2.

- **Step 4:**

Insertion of idling phases: a random set of idling intervals is created and inserted between the micro-cycles of the final selected candidate. This method was chosen for simplicity reasons, idling phases are not essential for the final energy consumption calculation of battery electric vehicles since the idling losses are minimal. (4.3) shows how they are created:  $\mathbf{s}$  represents a vector of  $m$  idling intervals where  $\mathbf{s} \in \mathbb{R}^{+,m \times 1}$ . Vector  $\mathbf{r}$  represents a random vector with normally distributed values  $\mathbf{r} \sim \mathcal{N}(\mu = 0, \sigma^2 = 1)$ , where  $\mathbf{r} \in \mathbb{R}^{m \times 1}$ . The sum of the intervals (4.4) has to equal the statistical mean idling time of the case study trips.  $m$  is the micro-cycle count minus one.

$$\mathbf{s} = \sigma_{idle} \cdot \mathbf{r} + \mu_{idle} \cdot \mathbb{1}_m \quad (4.3)$$

$$\frac{\sum_{i=1}^m s_i}{t_{DC}} = \frac{t_{idle\_overall}}{t_{overall}} \quad (4.4)$$

The same process is followed to generate a representative driving cycle with a limited speed of 25 km/h; the maximum permitted speed among several countries with specific regulations tailored to light electric vehicles.

The pool of micro-cycles used to generate random combinations is reduced to the MCs with a maximum speed equal or lower than the target.



# 5 Results

A total of 220 useful ride-logs (130 ride hours with an accumulated distance of 2000 km) were analyzed. The trips were segmented into 2800 micro-cycles of which 64 % had a maximum speed equal or lower than 25 km/h.

## 5.1 Driving Behavior

On the one hand, as can be observed from Figure 5.1, e-skateboards are mainly used for short and medium distance trips, which generally corresponds to typical urban commute distances. 65 % of the trips covered a distance of less than 10 km, the median value of the distance distribution being 6.54 km. The mean trip distance was 9.68 km with a standard deviation of 10.32 km.

On the other hand, 12 % of the trips were more prolonged than 20 km, proving that e-skateboards can also be used for longer commutes or occasional recreational long-distance trips.

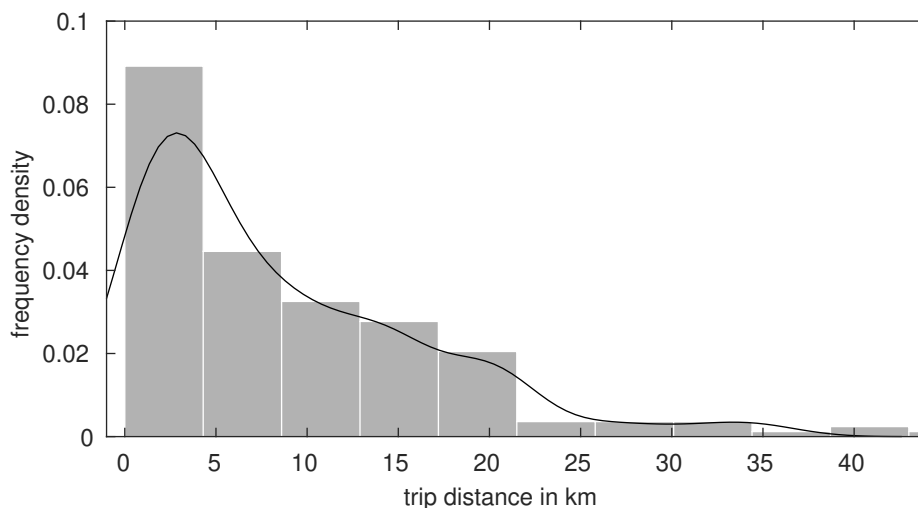


**Figure 5.1.** Trip distance distribution

The mean speed distribution can be observed in Figure 5.2. The average recorded value was 16 km/h with a standard deviation of 7.15 km/h. A vast group of cities in developed countries, like for instance Paris, Manchester or Chicago, exhibit a lower average traffic speed [30]. This circumstance is mainly caused by traffic retention, an occurrence that does not affect personal light electric mobility.

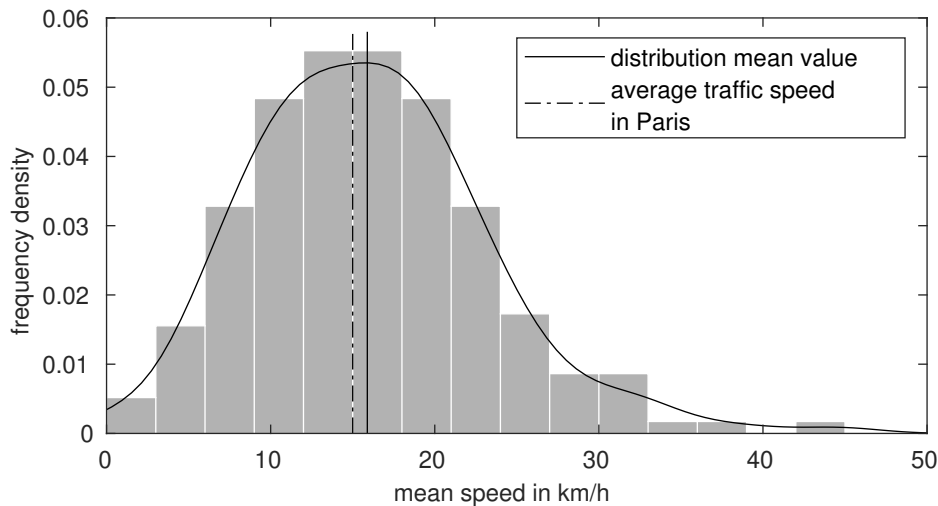


**Figure 5.2.** Mean trip speed

In Figure 5.3 the distribution of the maximum ride speed can be observed. The observed mean value of the distribution is 37 km/h, with a standard deviation of 9 km/h.

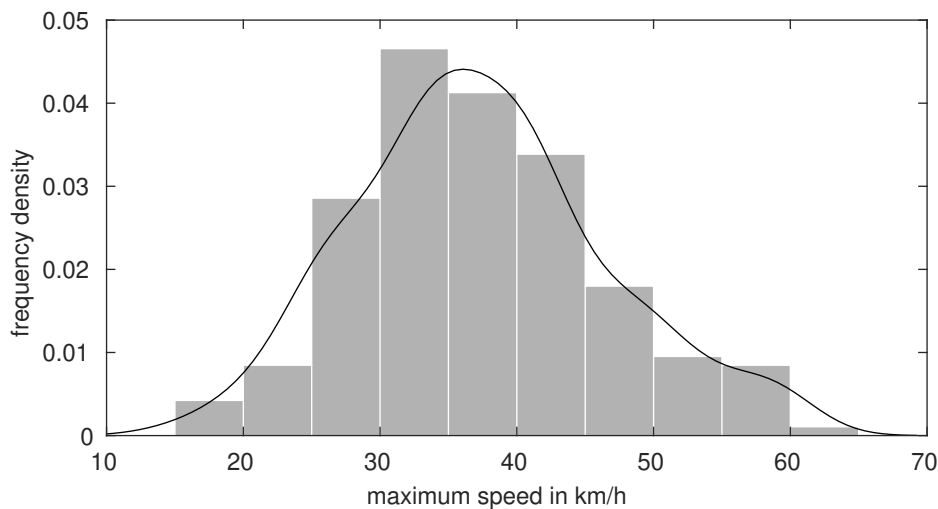


**Figure 5.3.** Maximum trip speed distribution

Figure 5.4 (a) shows the distribution of the cruising duration. The average time spent cruising is only 2.45 seconds, with a standard deviation of 2.06 seconds. This suggests that electric skateboard urban commuting is subjected to constant dynamic speed and acceleration changes which impede longer cruising situations.

Figure 5.4 (b) shows the distribution of the mean speed when cruising. A tendency to cruise at higher speeds, 20-35 km/h, can be observed from the function shape. This results meet the expectations since both ends of the speed spectrum are usually not maintained for a prolonged time. Higher speeds are usually not maintained for stability reasons, and lower speeds tend to be generally uninteresting for most riders. The recorded mean cruising speed is 22 km/h, with a standard deviation of 8 km/h. The 2 peaks at 25 and 31 km/h are a result of the low count of analyzed rides and do not possess any informative value.

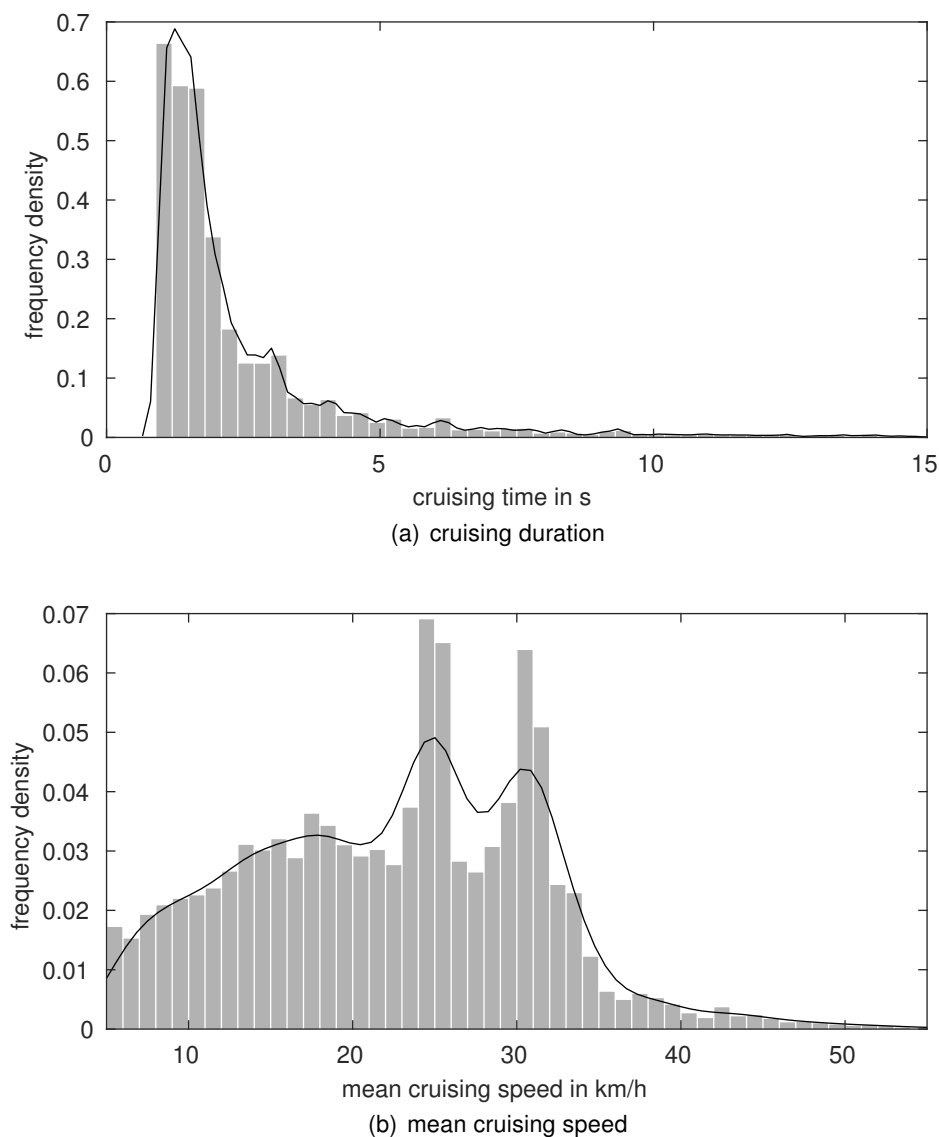


**Figure 5.4.** Cruising duration and speed

The heatmap in Figure 5.5 shows the normalized distribution of power over speed,  $v=0$  and  $P=0$  not being included in the represented data-set. A disparity between the positive and negative power spectrum can be observed. The cause for this phenomenon could be the charge current limitation of most battery setups. As mentioned in 2.2.1, lithium-ion batteries show an asymmetry in discharge and charge ratings, because of that, the ESC discharge and charge settings are also asymmetrically configured in order to preserve battery health.

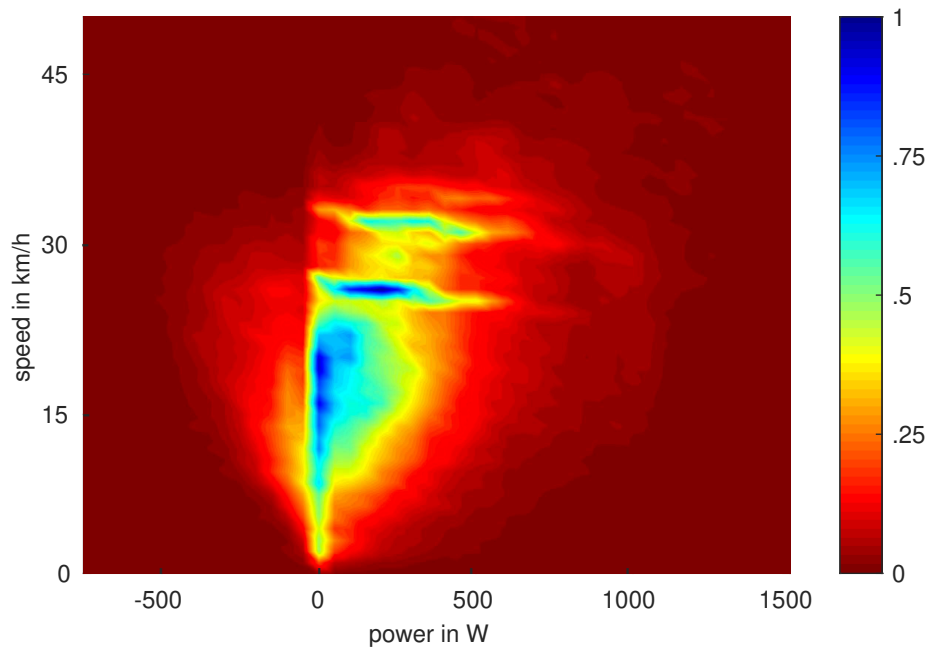


Figure 5.5. Power distribution linked to the ride speed

## 5.2 Use of Energy

Figure 5.6 shows the distribution of mean energy consumption. The average value of the distribution is 11.70 Wh/km with a standard deviation of 6.55 Wh/km. Because of the skewness of the distribution, the median value of 10.10 Wh/km should be seen as the reference value. That would result in an approximate energy consumption 20 times lower than an electric automobile under urban driving conditions with an average driving speed of 16 km/h [31].

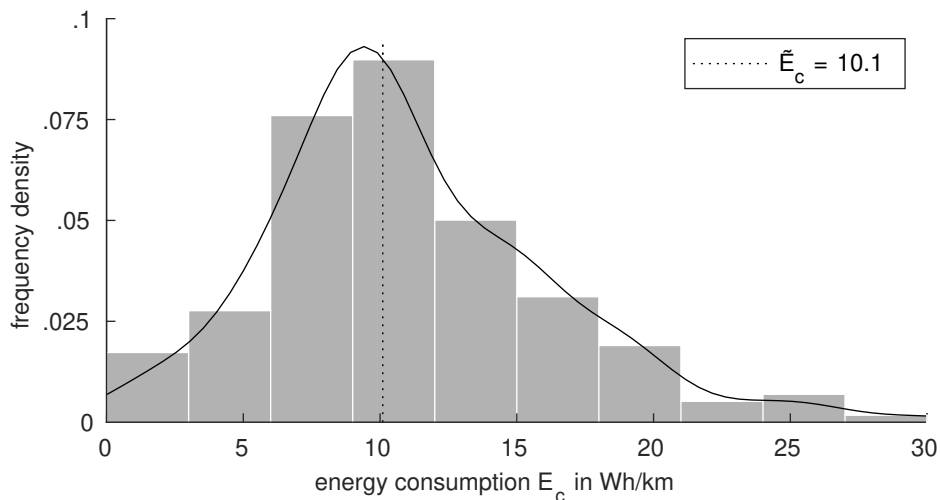
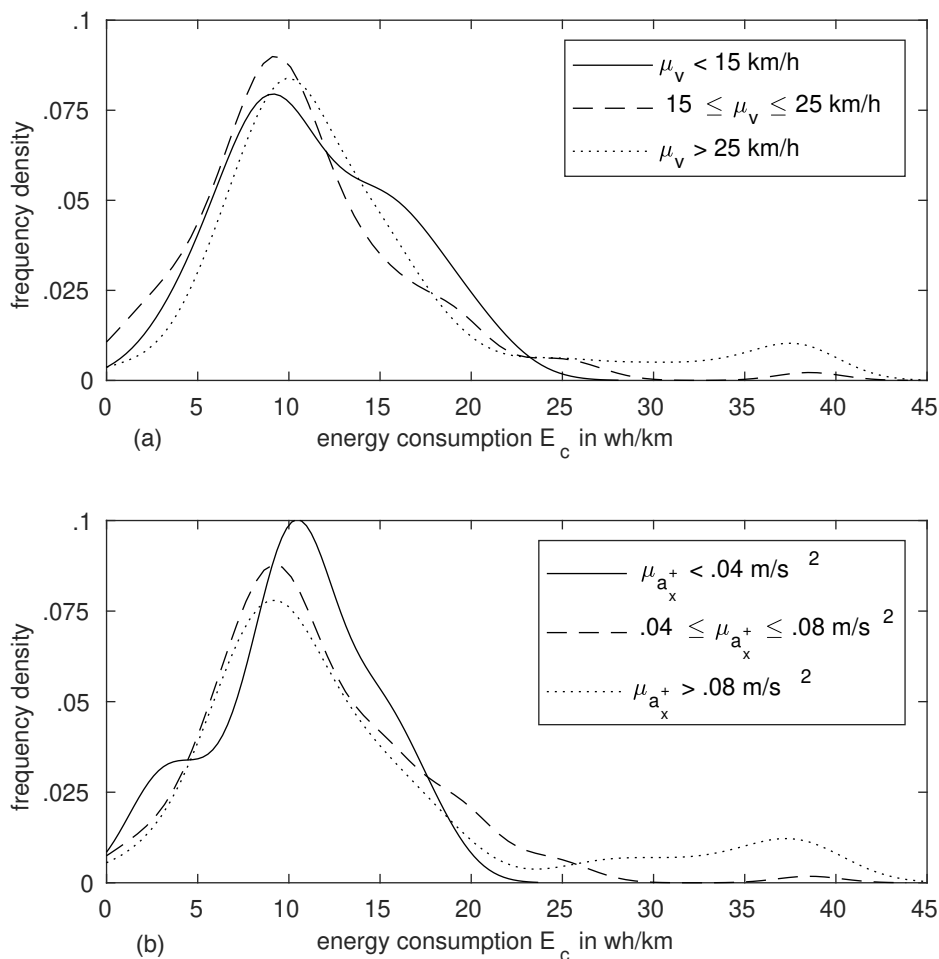


Figure 5.6. Normalized energy use histogram

Figure 5.7 (a) shows three consumption distributions grouped by the mean trip speed. In Figure 5.7 (b) the consumption distributions are grouped by the mean positive acceleration. The results suggest that other factors such as wheel diameter, rider weight or battery-configuration may have a greater impact than the acceleration and speed values alone. There cannot be observed any direct correlation between higher energy consumption and higher mean speed or greater positive acceleration values.



**Figure 5.7.** Top: rides grouped by mean speed (excl.  $v=0$ ) in km/h. Bottom: rides grouped by mean positive acceleration in  $m/s^2$

A similar phenomenon can be observed in Figure 5.8 were the database trips were segmented by the mean altitude gradient. There is no clear correlation between higher altitude changes and higher consumption values. Only the sub 3% gradient rides show a slightly wider distribution shape than the rest, although the mean value remains similar. Additionally a predominance of high consumption values over 30 Wh linked to the +6% gradient curve can be observed.

The sensibility analysis presented in Figure 5.7 and 5.8 has to be repeated with a higher count of collected rides to obtain a preciser statistical representation.

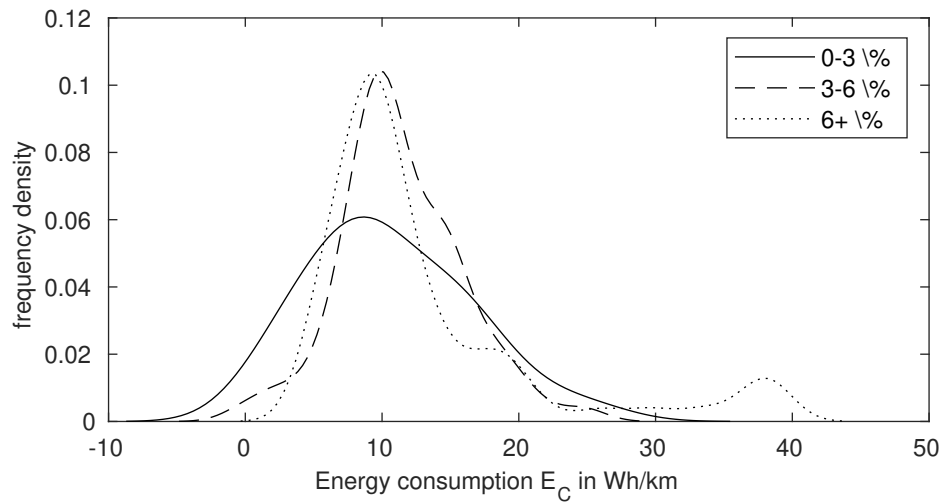


Figure 5.8. Effect of altitude change on energy consumption

### 5.3 Driving Cycle

Both proposed representative driving cycle candidates are shown in the following subsections; the data corresponding to the driving cycles can be found in Appendix A and B.

#### Non-Limited Driving Cycle

The non-limited driving cycle, consists of eight combined micro-cycles, which is the median number of the micro-cycles per trip distribution. It includes four long and four short intervals.

Being generated out of real-world data, it has a top speed of 43 km/h, which may exceed the maximum permitted speed of most countries. The total duration of the proposed DC is about 2000 seconds or 33 minutes, from which 8 minutes or 24 % correspond to idling time. It covers a total distance of 8.7 km with an average speed of 14.7 km/h; 19.3 km/h without idling time. The different properties of the non-limited driving cycle are listed in Table 5.1:

Table 5.1. Characteristics of the non-limited DC

Total time $t$ in s	1996
Idle time $t_{idle}$ in s	476
Distance $x$ in m	8695
Max. speed $v_{max}$ in km/h	43.58
Average speed $\mu_v, \forall v \in \mathbb{R}_0^+$ in km/h	14.68
Average speed $\mu_v, \forall v \in \mathbb{R}^+$ in km/h	19.29
Max. acceleration $a_x$ in $m/s^2$	1.01
Min. acceleration $a_x$ in $m/s^2$	-1.25

Figure 5.9 (a) shows the progression of speed over time, whilst image (b) shows the derivate of the discrete function above:

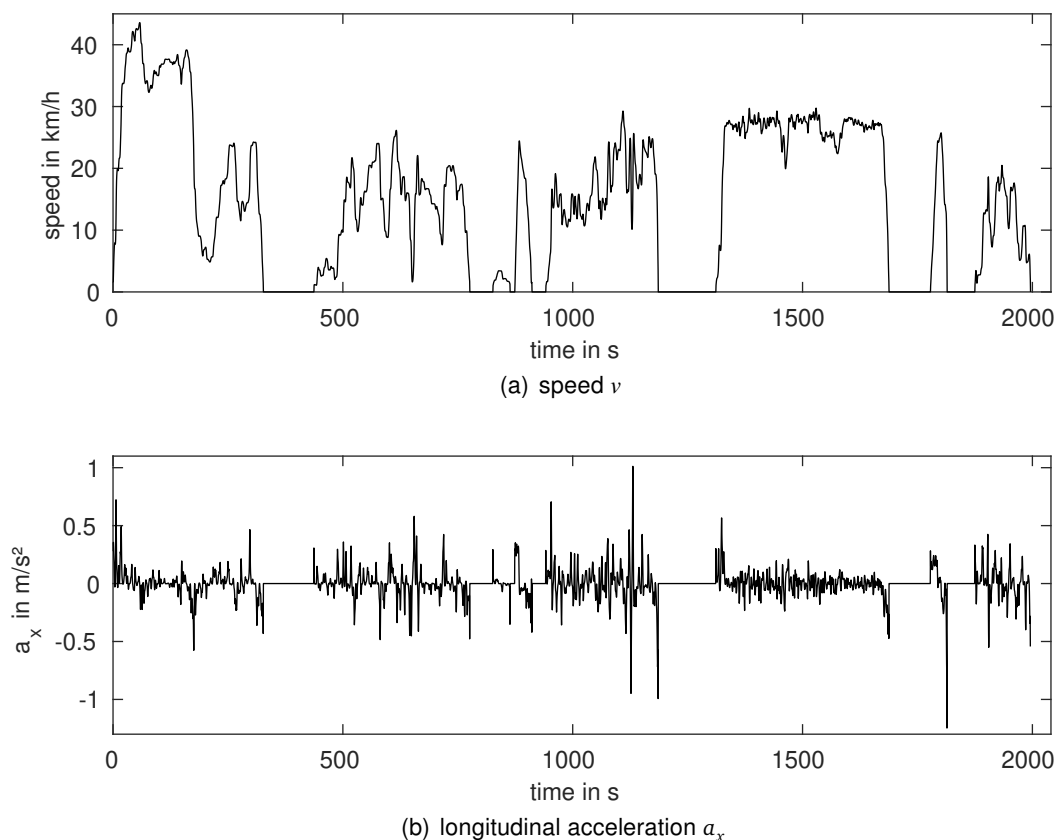


**Figure 5.9.** Non-limited driving cycle

Table 5.2 shows the comparison of the first reference values, listed as step 2 in section 4.3. The average deviation from the target values was 2.2%. A total of about 220 samples out of the one million generated were selected after the first sorting phase.

**Table 5.2.** First selection step (non-limited DC)

Data	Pearson Type $v$	$\mu_v$	$\sigma_v$	Pearson Type $a_x$	$\mu_{a_x^+}$	$\mu_{a_x^-}$	$RMS_{a_x}$	$\sigma_{a_x}$
Reference	1	5.346	2.704	4	0.076	-0.077	0.129	0.129
Candidate	1	5.354	2.718	4	0.081	-0.078	0.129	0.129

Table 5.3 shows the comparison of the operating mode proportions. The added total difference was only 0.03%.

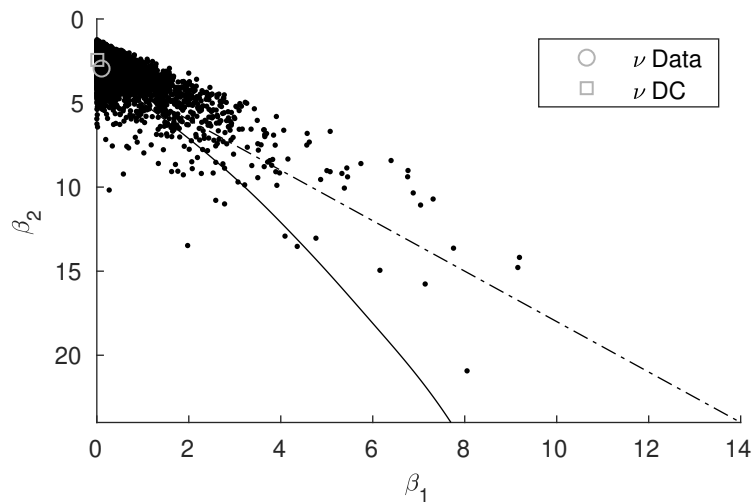
**Table 5.3.** Second selection step (non-limited DC)

Data	% creep	% cruise	% accel.	% decel.	Added Difference
Reference	3.747 %	15.227 %	40.26 %	40.766 %	0.0317 %
Candidate	3.747 %	15.227 %	40.26 %	40.765 %	

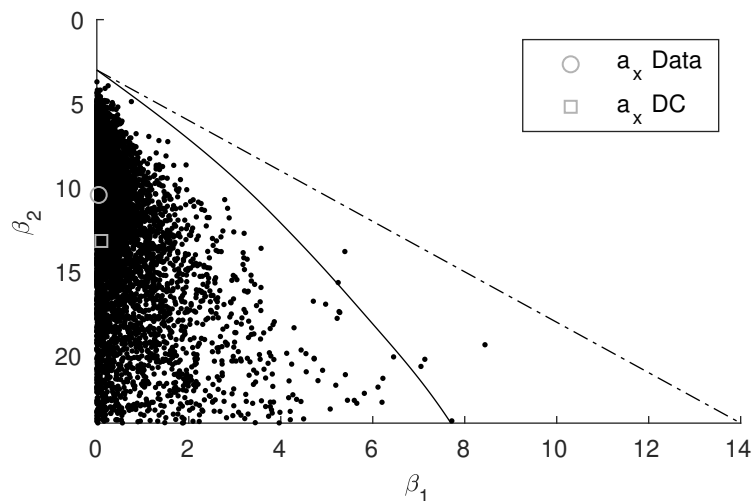
In Figure 5.10 the  $\beta_1$  and  $\beta_2$  Pearson distribution system values of  $10^3$  random candidate driving cycles were plotted. Figure 5.10 (a) represents the Pearson speed distribution type, whilst (b) represents the acceleration distribution type of the candidate DCs. The Pearson distribution and its different distribution types are described in section 3.

The speed and acceleration distribution types of the collected data and the final DC-candidate are also shown in Figure 5.10 labeled with a round marker and a square marker respectively.

In 5.10 (b) it can be observed that nearly all (93.78 %) of the candidate DC distribution types represent the Pearson type IV. In contrast, image (a) shows a more divers dispersion of the candidate DC speed distribution types, ranging form Pearson type I to VI. By applying the Pearson distribution filtering to the driving cycle generation, a lot of candidate DCs with notably different data distributions could be filtered out.



(a)  $\nu$  Pearson diagram distribution



(b)  $a_x$  Pearson diagram distribution

**Figure 5.10.** Pearson speed and acceleration data distribution

Figure 5.11 shows the distribution curve of the collected data and the final DC candidate. Image (a) shows the speed data distribution comparison whilst image (b) shows the acceleration distribution comparison. Relatively similar data progressions can be observed for the speed and acceleration curves; this suggests a satisfactory data representation of the presented DC.



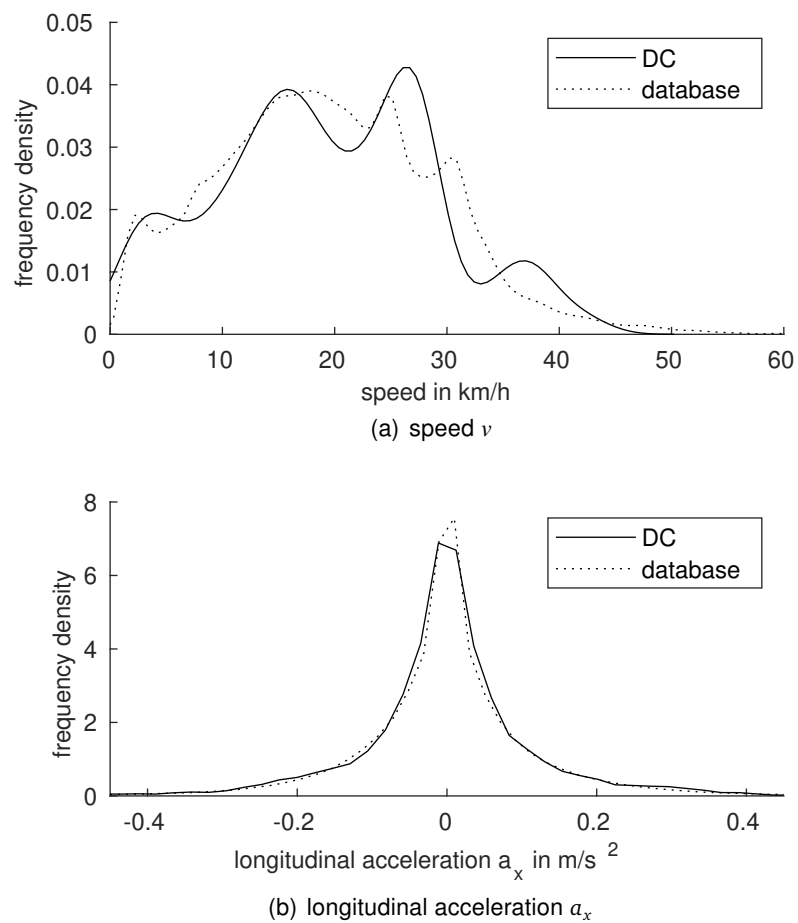


**Figure 5.11.** Database and candidate driving cycle distribution shape comparison

Finally, Figure 5.12 shows the probability distribution of the correlation between speed and acceleration data points of the real world recorded data (left), and the proposed driving cycle (right). Similar probability distributions can be observed between the two heatmaps, even a comparable peak around 30 km/h.

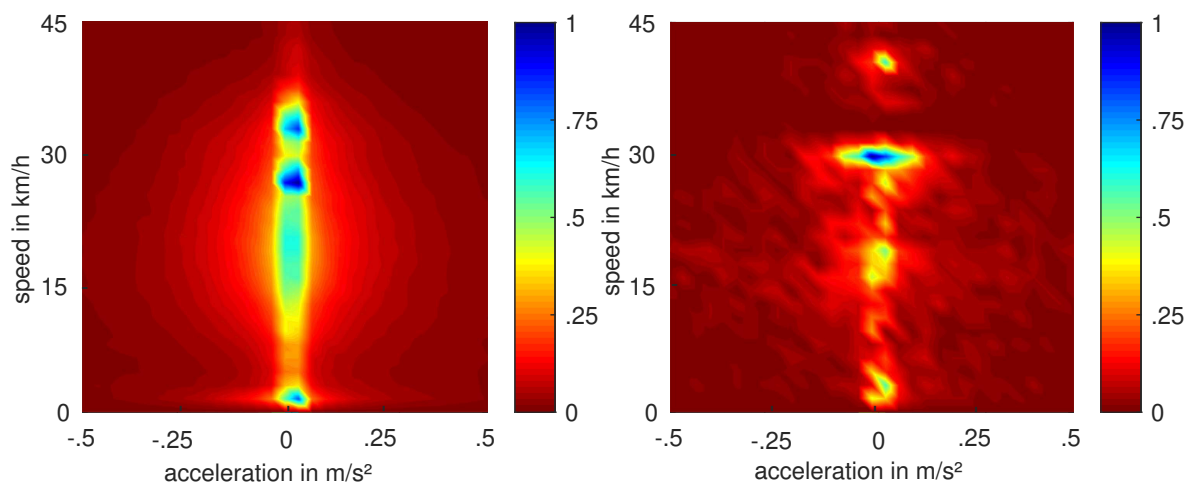


**Figure 5.12.** Speed-acceleration probability distribution: general vs proposed DC

## Limited Speed Driving Cycle

The proposed limited speed driving cycle consists like the non limited one of a combination of eight micro-cycles; three long and five short driving intervals.

The top speed of this DC is 23.2 km/h and it covers a total length of about 3 km in 20 minutes, 10 minutes less than the non-limited driving cycle. The mean speed is 9 km/h, 12 km/h without idle phases. It also shows a lower maximum positive acceleration than its counterpart. The idle phase was synthetically generated to equal the same proportion of the total time as the non-limited driving cycle: 24 %. The different properties of the limited-speed driving cycle are listed in Table 5.4:

**Table 5.4.** Characteristics of the 25 km/h limited DC

Total Time $t$ in s	1175
Idle Time $t_{idle}$ in s	281
Distance $x$ in m	2942
Max. Speed $v_{max}$ in km/h	23.19
Average Speed $\mu_v, \forall v \in \mathbb{R}_0^+$ in km/h	9.02
Average Speed $\mu_v, \forall v \in \mathbb{R}^+$ in km/h	11.85
Max. Acceleration $a_x$ in $m/s^2$	0.45
Min. Acceleration $a_x$ in $m/s^2$	-1.18

Figure 5.13 (a) shows the progression of speed over time of the selected final DC candidate, whilst image (b) shows the progression of the acceleration values.

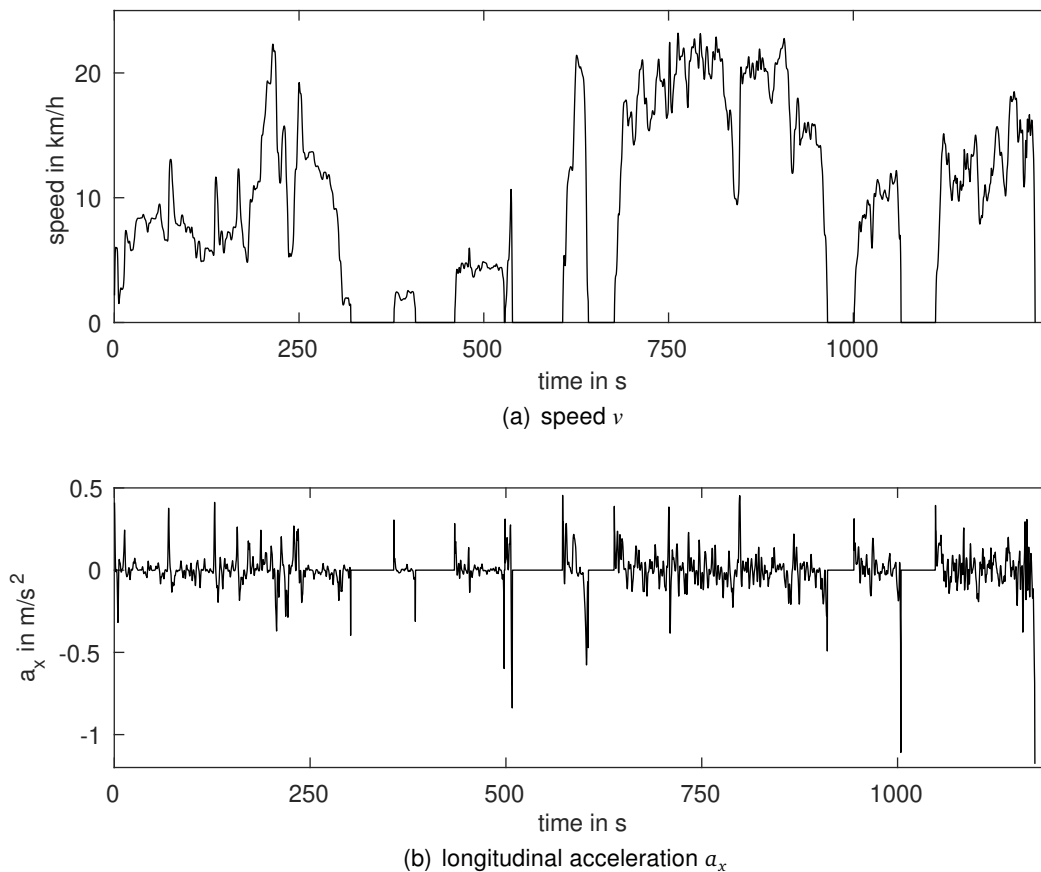


**Figure 5.13.** 25 km/h limited speed driving cycle

Table 5.5 compares the first eight filtering parameters: Pearson speed distribution type, mean speed, speed standard deviation, distribution type of the longitudinal acceleration, mean positive and negative acceleration, acceleration root mean square, and acceleration standard deviation. The average deviation from the target values was 8 %.

**Table 5.5.** First selection step (25 km/h limited DC)

Data	Pearson Type $\nu$	$\mu_\nu$	$\sigma_\nu$	Pearson Type $a_x$	$\mu_{a_x^+}$	$\mu_{a_x^-}$	$RMS_{a_x}$	$\sigma_{a_x}$
Reference	1	3.295	1.635	4	0.066	-0.068	0.114	0.114
Candidate	1	3.287	1.654	4	0.060	-0.060	0.101	0.101

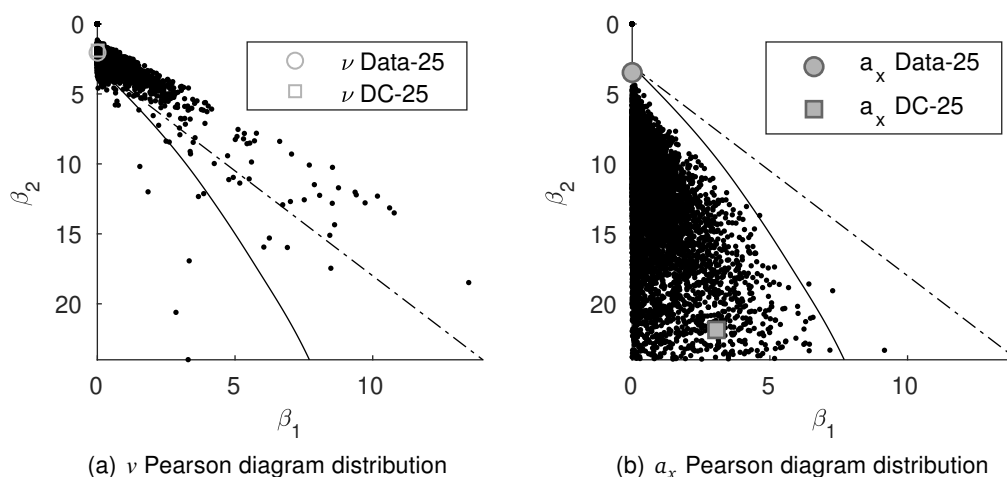
Table 5.6 compares the operating mode proportions over the cycle. The added total difference from the target values was 2.79 %.

**Table 5.6.** Second selection step (25 km/h limited DC)

Data	% creep	% cruise	% accel.	% decel.	Added Difference
Reference	8.725 %	13.714 %	38.276 %	39.285 %	2.79 %
Candidate	9.164 %	14.677 %	38.062 %	38.097 %	

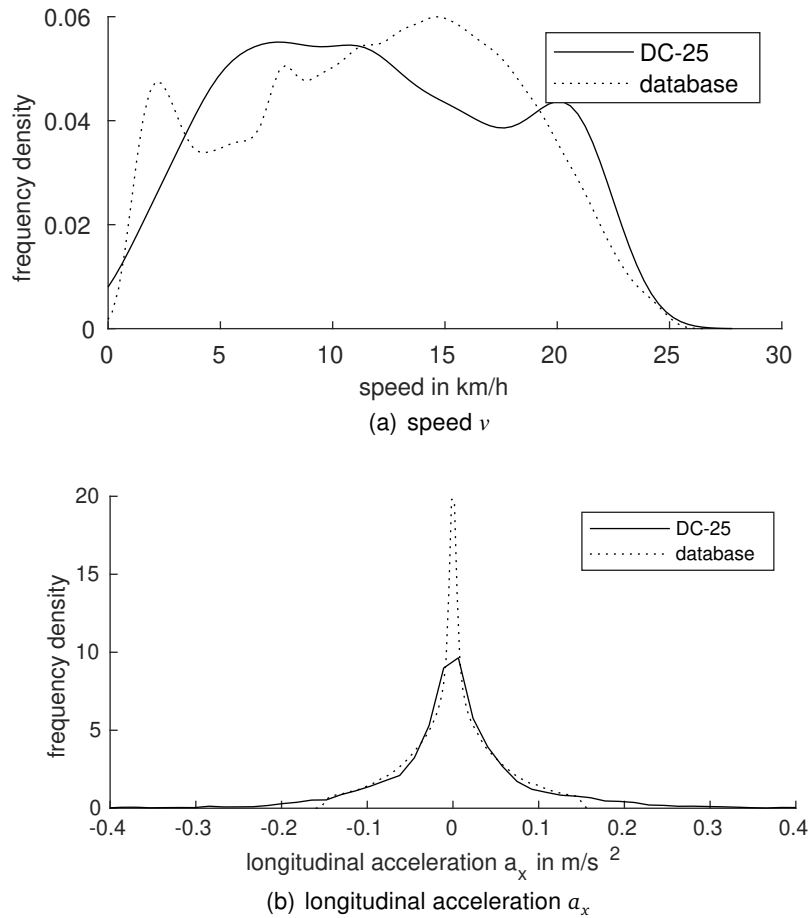
Figure 5.14 shows the Pearson distribution types of  $10^3$  random DC candidates. Figure 5.14 (a) represents the speed distribution type, whilst (b) represents the acceleration data distribution type. Analogue to the data presented for the non-limited driving cycle in Figure 5.10, the Pearson distribution type filtering is proven to be useful when observing the higher dispersion of the speed data distribution types. In contrast, 83,68 % of the longitudinal acceleration distribution types represent the Pearson type IV, with some exceptions of type VI.

The speed and acceleration distribution types of the collected data and the final DC-candidate are also shown in Figure 5.14 labeled with a round marker and a square marker respectively.



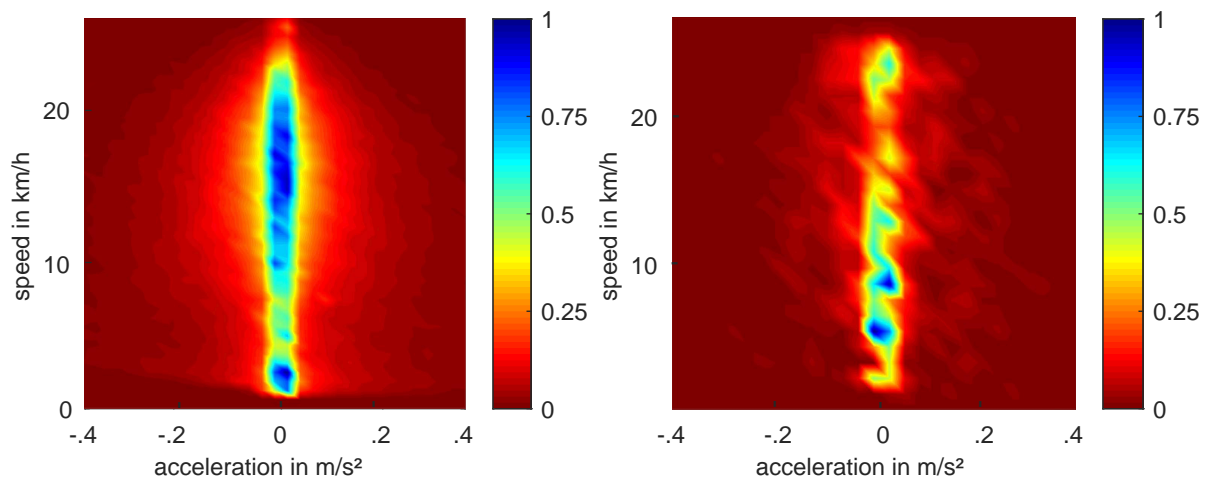
**Figure 5.14.** Pearson speed and acceleration data distribution

Figure 5.15 shows the distribution curve of the collected data and the final DC candidate. Image (a) shows the speed data distributions whilst image (b) shows the acceleration data distributions. The speed distribution follows the trend-line of the collected data, whilst the acceleration distribution curve exhibits lower probability density peak. This phenomenon may be caused because of the overall data point count difference between the collected data and the candidate driving cycle: a higher count of greater absolute acceleration values may stretch the distribution shape of the collected data, consequently generating a sharper function shape.



**Figure 5.15.** Database and candidate driving cycle distribution shape comparison

Finally, Figure 5.16 shows the normalized speed and acceleration correlation distribution of the collected data (left) and the proposed driving cycle (right). A comparable value dispersion can be observed. It has to be kept in mind that there is a large data-point difference between the general distribution and the 20-minute-long driving cycle, which may cause a shift in peak value regions: fewer data-points provoke a more inhomogeneous distribution across the heatmap.



**Figure 5.16.** Speed-acceleration probability distribution: general vs. proposed DC



## 6 Discussion

Some aspects should be considered for the further development of content based on this thesis:

- **Representativeness of the statistical analysis:**

More data would be required in order to obtain a more accurate representation of the presented results as well as a to improve the presented driving cycles. More complex sensibility analysis could also be done with more telemetry data. By analyzing the effect on energy consumption of driving aggressivity, speed, driving modes and altitude change, energy consumption conversion factors could be developed for a more accurate range estimation.

The data source has to be also kept in mind when observing the presented results: all case study participants are members of a community of *do-it-yourself* (DIY) electric skateboard builders [5], this implies that the driven e-skateboards provide a a speed and power spectrum significantly larger than most commercial e-skateboards do. This fact does not compromise the presented data, since the main goal is to observe the usage of e-skateboards in a non electrically constrained environment.

- **General representativeness of the driving cycles:**

More iterations would be required to increase the decision-making tolerance. Increased data storage and computing power would be needed. A target goal would be to generate one hundred million samples of each driving cycle: This decision is based on the work presented by Pfirheim et al. on the development of real-world Driving-Cycles for Battery Electric Vehicles [19]. Additionally, the Pearson distribution  $\beta_1$  and  $\beta_2$  values of the collected data and the driving cycle candidates could be compared to get a better estimation of the speed and acceleration distribution shape.

Another option would be to implement a 2 dimensional distribution type analyzing technique, that would mean that the speed and acceleration correlation would be compared directly. High positive accelerations and lower negative acceleration values may be linked to lower ride speeds, whilst low positive and high negative acceleration values might be linked to higher driving speeds. This correlation can not be shown in one dimensional distribution analyzers such as the Pearson distribution system.

- **Non-limited driving-cycle:**

Analyzing the response of real-world testing under the presented driving cycle conditions would be necessary to verify its effectiveness and representativeness. The verification under test bench conditions would also be recommendable.

- **Representativeness of the limited speed driving cycle:**

Due to the fact that the e-skateboards used in this case study had no electronic speed limitation, a different driving-strategy is expected from riders using boards which do have a mandatory speed limit. This theory would have to be tested under real-world conditions to be corroborated. Based on the results presented in this thesis higher top speed cruising proportions are expected since the drivers would not be able to surpass the mandatory speed limitation.



# 7 Conclusion

This thesis presented some insight into the real-world use of electric skateboards. The usage variety and potential as an alternative mobility device can be observed, thus proving that e-skateboards can help omit the need for a personal car or public transportation in everyday situations. The portability of e-skateboards allows for a new form of combined mobility, as they are easily transported in a car, bus, or train. The presented results also demonstrate that e-skateboards can be used for long distance commutes. A large proportion of the recorded trips exhibit an end-distance that exceeds 20 km.

The observed trip distance distribution indicates that most commercially available e-skateboards potentially have an under-dimensioned battery solution, often ranging from 99 Wh to 250 Wh. Considering typical depth of discharge (DoD) values of 20 to 30 % and driving factors such as rider weight, driving aggressivity or altitude change, only short distance commutes seem feasible.

Two different driving cycles were presented: they represent the dynamics and usage of real-world riding and have the potential to be utilized as a universal range determining tool. They also provide a universal platform for product development and testing. In addition to the collected anonymous database, the driving cycle results found in Appendix A and B will remain accessible to any person or group that may want to further investigate other aspects related to electric skateboarding, thereby expanding the scientific foundation. Electric-skateboarding is a relatively new concept and consequently open scientific literature remains limited.



# List of Figures

Figure 2.1:	Electric skateboard .....	4
Figure 2.2:	VESC design: left: V6; right: V4 .....	5
Figure 2.3:	ENERTION® direct drive hubmotor. ....	7
Figure 2.4:	RKP truck kinematics .....	7
Figure 3.1:	Pearson system distribution types.....	13
Figure 4.1:	Overall process of the case study approach .....	15
Figure 4.2:	Data localization .....	16
Figure 4.3:	E-Mail scraper program work-flow.....	17
Figure 4.4:	Speed data fitting.....	18
Figure 4.5:	Micro-Cycles .....	19
Figure 5.1:	Trip distance distribution .....	23
Figure 5.2:	Mean trip speed.....	24
Figure 5.3:	Maximum trip speed distribution .....	24
Figure 5.4:	Cruising duration and speed .....	25
Figure 5.5:	Power distribution linked to the ride speed.....	26
Figure 5.6:	Normalized energy use histogram.....	26
Figure 5.7:	Top: rides grouped by mean speed (excl. $v=0$ ) in km/h. Bottom: rides grouped by mean positive acceleration in $m/s^2$ .....	27
Figure 5.8:	Effect of altitude change on energy consumption .....	28
Figure 5.9:	Non-limited driving cycle .....	29
Figure 5.10:	Pearson speed and acceleration data distribution.....	30
Figure 5.11:	Database and candidate driving cycle distribution shape comparison .....	31
Figure 5.12:	Speed-acceleration probability distribution: general vs proposed DC .....	31
Figure 5.13:	25 km/h limited speed driving cycle.....	32
Figure 5.14:	Pearson speed and acceleration data distribution.....	33
Figure 5.15:	Database and candidate driving cycle distribution shape comparison .....	34
Figure 5.16:	Speed-acceleration probability distribution: general vs. proposed DC .....	35



# List of Tables

Table 4.1: Overview of the parameters used for the DC-generation ..... 20

Table 4.2: Operating mode determination boundaries..... 21

Table 5.1: Characteristics of the non-limited DC ..... 28

Table 5.2: First selection step (non-limited DC) ..... 29

Table 5.3: Second selection step (non-limited DC) ..... 29

Table 5.4: Characteristics of the 25 km/h limited DC ..... 32

Table 5.5: First selection step (25 km/h limited DC)..... 33

Table 5.6: Second selection step (25 km/h limited DC) ..... 33



# Bibliography

- [1] EEA, „Air quality in Europe - 2018 report,“ European Environment Agency, 2018.
- [2] WHO, „Air quality guidelines - global update 2005,“ World Health Organization, 2005.
- [3] S. Sahlqvist et al., „Change in active travel and changes in recreational and total physical activity in adults: longitudinal findings from the iConnect study,“ *International Journal of Behavioral Nutrition and Physical Activity*, vol. 10, no. 1, p. 28, 2013.
- [4] J. D. Bishop et al., „Investigating the technical, economic and environmental performance of electric vehicles in the real-world: A case study using electric scooters,“ *Journal of Power Sources*, vol. 196, no. 23, pp. 10094–10104, 2011.
- [5] „. Electric skateboard builders forum,“ <https://www.electric-skateboard.builders/>. 2018.
- [6] R. W. Goodman, „Whatever you call it, just don't think of last-mile logistics, last,“ *Global Logistics & Supply Chain Strategies*, vol. 9, no. 12, pp. 46–51, 2005.
- [7] „. VESC – Open Source ESC,“ <https://github.com/vedderb/bldc-hardware>. 2018.
- [8] „. Source code for the VESC DC/BLDC/FOC controller,“ <https://github.com/vedderb/bldc>. 2018.
- [9] K. H. Nam, *AC motor control and electric vehicle applications*, CRC press, 2010, isbn: 9781439819630.
- [10] X. Yuan et al., *Lithium-ion batteries: advanced materials and technologies*, CRC press, 2016.
- [11] M. Zigliotto. „Permanent magnet synchronous motor drives,“ in: *Power Electronic Converters and Systems: Frontiers and Applications*. Institution of Engineering and Technology, 2016. Chap. 10, pp. 313–332.
- [12] S. T. Agency. „TSFS 2009: 31,“ October 10, 2010.
- [13] M. of Transport and C. of Finland. „Vehicles Act 190/2002; amendments up to 402/2005 included,“ 2006.
- [14] G. o. S. Land Transport Authority. „Active Mobility Bill,“ January 10, 2017.
- [15] State of California. „Assembly Bill No. 604 - Electrically motorized boards,“ October 11, 2015.
- [16] U. N. E. C. for Europe. „New European Driving Cycle (NEDC),“ 1997.
- [17] U. N. E. C. for Europe. „Worldwide harmonized Light vehicles Test Procedure (WLTP),“ Jun 13, 2012.
- [18] U. E. P. Agency. „US: Light-duty Federal Test Procedure: FTP-75,“ 2008.
- [19] M. Pfriem and F. Gauterin, „Development of real-world Driving Cycles for Battery Electric Vehicles,“ *World Electric Vehicle Journal*, vol. 8, no. 1, pp. 14–24, 2016.

- [20] V. Schwarzer and R. Ghorbani, „Drive Cycle Generation for Design Optimization of Electric Vehicles.“ *IEEE Trans. Vehicular Technology*, vol. 62, no. 1, pp. 89–97, 2013.
- [21] Y. Yang et al., „Markov chain-based approach of the driving cycle development for electric vehicle application,“ *Energy Procedia*, vol. 152, pp. 502–507, 2018.
- [22] K. Pearson, „Contributions to the mathematical theory of evolution. II. Skew variation in homogeneous material,“ *Philosophical Transactions of the Royal Society of London*, vol. 186, no. Part I, pp. 343–424, 1895.
- [23] D. C. Montgomery and G. C. Runger, *Applied statistics and probability for engineers*, John Wiley & Sons, 2010.
- [24] E. S. Pearson, „Some problems arising in approximating to probability distributions, using moments,“ *Biometrika*, vol. 50, no. 1/2, pp. 95–112, 1963.
- [25] D. Sanderson, *Programming google app engine: build and run scalable web apps on google's infrastructure*, " O'Reilly Media, Inc.", 2009.
- [26] „ VLDA – VESC® Data log analyzer,“ <https://www.gct-hp.de/VDLA/>. 2018.
- [27] W. T. Hung et al., „Development of a practical driving cycle construction methodology: A case study in Hong Kong,“ *Transportation Research Part D: Transport and Environment*, vol. 12, no. 2, pp. 115–128, 2007.
- [28] H. Tong et al., „Development of a driving cycle for Hong Kong,“ *Atmospheric Environment*, vol. 33, no. 15, pp. 2323–2335, 1999.
- [29] T. J. BARLOW et al., „A reference book of driving cycles for use in the measurement of road vehicle emissions,“ *TRL Published Project Report*, 2009.
- [30] INRIX®, „INRIX Global Traffic Scorecard - 2017 report,“ 2018.
- [31] F Badin et al., „Evaluation of EVs energy consumption influencing factors, driving conditions, auxiliaries use, driver's aggressiveness,“ *World Electric Vehicle Journal*, vol. 6, no. 1, pp. 112–123, 2013.



# Appendix

**A Appendix A ..... ix**  
**B Appendix B ..... xv**

























10.74, 10.81, 10.88, 10.94, 10.99, 11.03, 11.06, 11.07, 11.08, 11.1, 11.1, 11.11, 11.13, 11.14, 11.16, 11.21, 11.26, 11.34, 11.45, 11.57, 11.71, 11.88, 12.05, 12.19, 12.31, 12.38, 12.38, 12.35, 12.3, 12.21, 12.13, 12.06, 11.98, 11.91, 11.86, 11.81, 11.78, 11.78, 11.79, 11.8, 11.84, 11.88, 11.92, 11.97, 12.03, 12.07, 12.11, 12.16, 12.18, 12.21, 12.26, 12.29, 12.33, 12.39, 12.45, 12.51, 12.6, 12.69, 12.79, 12.9, 13.01, 13.1, 13.2, 13.31, 13.39, 13.48, 13.59, 13.67, 13.75, 13.85, 13.93, 14.01, 14.11, 14.2, 14.29, 14.4, 14.52, 14.64, 14.77, 14.9, 14.99, 15.07, 15.15, 15.21, 15.26, 15.33, 15.39, 15.44, 15.5, 15.54, 15.57, 15.6, 15.63, 15.64, 15.66, 15.68, 15.68, 15.69, 15.71, 15.7, 15.7, 15.7, 15.68, 15.65, 15.64, 15.61, 15.58, 15.57, 15.55, 15.52, 15.5, 15.47, 15.43, 15.39, 15.35, 15.29, 15.24, 15.19, 15.11, 15.05, 14.99, 14.91, 14.83, 14.76, 14.67, 14.57, 14.48, 14.38, 14.26, 14.15, 14.05, 13.93, 13.83, 13.75, 13.66, 13.58, 13.53, 13.47, 13.42, 13.4, 13.39, 13.38, 13.39, 13.41, 13.43, 13.46, 13.5, 13.53, 13.56, 13.6, 13.61, 13.63, 13.65, 13.64, 13.63, 13.63, 13.6, 13.57, 13.54, 13.49, 13.43, 13.38, 13.31, 13.24, 13.16, 13.09, 13, 12.91, 12.84, 12.73, 12.64, 12.55, 12.45, 12.36, 12.27, 12.18, 12.09, 12, 11.91, 11.82, 11.73, 11.65, 11.56, 11.48, 11.42, 11.34, 11.27, 11.22, 11.16, 11.1, 11.07, 11.02, 10.97, 10.94, 10.9, 10.85, 10.82, 10.78, 10.72, 10.67, 10.61, 10.53, 10.45, 10.38, 10.29, 10.22, 10.18, 10.14, 10.12, 10.13, 10.16, 10.19, 10.25, 10.32, 10.39, 10.48, 10.58, 10.68, 10.8, 10.94, 11.07, 11.22, 11.39, 11.55, 11.7, 11.85, 11.98, 12.09, 12.2, 12.28, 12.34, 12.4, 12.46, 12.51, 12.58, 12.67, 12.76, 12.87, 13.01, 13.16, 13.33, 13.52, 13.72, 13.93, 14.16, 14.39, 14.61, 14.84, 15.06, 15.25, 15.44, 15.62, 15.77, 15.93, 16.09, 16.22, 16.35, 16.49, 16.6, 16.72, 16.84, 16.95, 17.06, 17.19, 17.32, 17.44, 17.56, 17.68, 17.77, 17.85, 17.94, 17.98, 18.03, 18.08, 18.1, 18.12, 18.14, 18.14, 18.12, 18.11, 18.09, 18.05, 18.01, 17.97, 17.91, 17.87, 17.84, 17.79, 17.76, 17.74, 17.71, 17.7, 17.71, 17.71, 17.73, 17.76, 17.78, 17.79, 17.82, 17.83, 17.83, 17.84, 17.85, 17.83, 17.84, 17.86, 17.87, 17.9, 17.97, 18.01, 18.08, 18.16, 18.22, 18.27, 18.33, 18.38, 18.41, 18.45, 18.49, 18.49, 18.5, 18.51, 18.47, 18.43, 18.4, 18.33, 18.26, 18.21, 18.14, 18.08, 18.04, 17.99, 17.95, 17.93, 17.92, 17.89, 17.89, 17.87, 17.87, 17.88, 17.87, 17.88, 17.91, 17.92, 17.94, 17.98, 17.99, 17.98, 17.96, 17.91, 17.82, 17.71, 17.58, 17.41, 17.23, 17.04, 16.82, 16.59, 16.37, 16.11, 15.86, 15.63, 15.4, 15.18, 15, 14.84, 14.71, 14.61, 14.55, 14.49, 14.46, 14.46, 14.44, 14.45, 14.48, 14.49, 14.52, 14.58, 14.62, 14.68, 14.75, 14.8, 14.85, 14.91, 14.97, 15.02, 15.1, 15.19, 15.27, 15.38, 15.5, 15.61, 15.75, 15.9, 16.01, 16.13, 16.23, 16.28, 16.29, 16.27, 16.19, 16.06, 15.92, 15.77, 15.62, 15.49, 15.39, 15.3, 15.24, 15.21, 15.18, 15.18, 15.2, 15.22, 15.24, 15.26, 15.26, 15.25, 15.25, 15.26, 15.27, 15.3, 15.34, 15.37, 15.4, 15.43, 15.44, 15.43, 15.39, 15.28, 15.09, 14.82, 14.46, 14.03, 13.58, 13.13, 12.69, 12.31, 11.98, 11.7, 11.49, 11.33, 11.18, 11.07, 10.99, 10.91, 10.87, 10.87, 10.87, 10.9, 10.95, 11.01, 11.07, 11.14, 11.23, 11.32, 11.45, 11.63, 11.82, 12.06, 12.35, 12.64, 12.98, 13.34, 13.69, 14.02, 14.31, 14.51, 14.62, 14.63, 14.53, 14.35, 14.13, 13.9, 13.66, 13.46, 13.31, 13.2, 13.17, 13.21, 13.31, 13.48, 13.72, 14, 14.33, 14.71, 15.1, 15.48, 15.82, 16.08, 16.24, 16.31, 16.3, 16.2, 16.07, 15.93, 15.76, 15.62, 15.51, 15.4, 15.32, 15.29, 15.26, 15.27, 15.31, 15.37, 15.46, 15.58, 15.73, 15.87, 16.04, 16.21, 16.35, 16.48, 16.61, 16.67, 16.7, 16.68, 16.59, 16.46, 16.29, 16.11, 15.91, 15.73, 15.57, 15.41, 15.28, 15.18, 15.08, 15.02, 15.01, 14.99, 15.01, 15.07, 15.13, 15.22, 15.34, 15.45, 15.56, 15.68, 15.79, 15.88, 15.98, 16.06, 16.12, 16.18, 16.23, 16.24, 16.24, 16.22, 16.18, 16.12, 16.07, 15.98, 15.89, 15.77, 15.62, 15.45, 15.26, 15.06, 14.86, 14.67, 14.49, 14.32, 14.18, 14.06, 13.95, 13.83, 13.69, 13.51, 13.32, 13.12, 12.9, 12.63, 12.28, 11.85, 11.39, 10.96, 10.56, 10.11, 9.55, 8.84, 8.05, 7.34, 6.77, 6.26, 5.62, 4.63, 3.25, 1.73, 0.45, 0, 0, 0